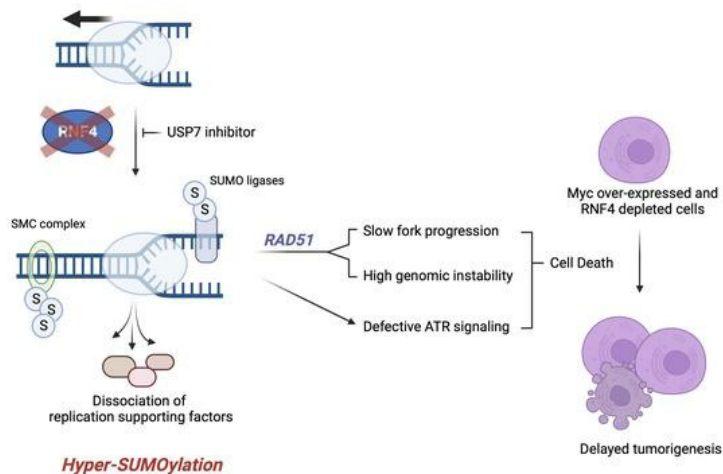# RNF4 sustains Myc-driven tumorigenesis by facilitating DNA replication

Joonyoung Her, … , Haiyan Zheng, Samuel F. Bunting

Research In-Press Preview Genetics Oncology

Graphical abstract

1   RNF4 sustains Myc-driven tumorigenesis by facilitating DNA replication

2

3   Joonyoung Her[1], Haiyan Zheng[2], and Samuel F. Bunting[1, *]

4

5   1. Department of Molecular Biology and Biochemistry, Rutgers, The State University of New

6   Jersey, Piscataway, NJ, USA.

7

8   2. Biological Mass Spectrometry Facility, Rutgers, The State University of New Jersey,

9   Piscataway, NJ, USA.

10

11

12   * Corresponding author:

13   Samuel F. Bunting

14   Center for Advanced Biotechnology and Medicine, Rutgers, The State University of New Jersey,

15   679 Hoes Lane West, Piscataway, NJ 08854, USA.

16   848.445.9894

17   bunting@cabm.rutgers.edu

18

19

20   Conflict-of-interest statement: The authors have declared that no conflict of interest exists.

21

22

23   Abstract

24

25   The mammalian SUMO-targeted E3 Ubiquitin Ligase, *Rnf4*, has been reported to act as a regulator

26   of DNA repair, but the importance of RNF4 as a tumor suppressor has not been tested. Using a

27   conditional-knockout mouse model, we deleted *Rnf4* in the B cell lineage to test the importance of

28   RNF4 for growth of somatic cells. Although *Rnf4* conditional-knockout B cells exhibited

29   substantial genomic instability, *Rnf4* deletion caused no increase in tumor susceptibility. In

30   contrast, *Rnf4* deletion extended the healthy lifespan of mice expressing an oncogenic c-*myc*

31   transgene. *Rnf4* activity is essential for normal DNA replication, and in its absence, there was a

32   failure in ATR-CHK1 signaling of replication stress. Factors that normally mediate replication

33   fork stability, including members of the Fanconi Anemia gene family and the helicases, PIF1 and

34   RECQL5, showed reduced accumulation at replication forks in the absence of RNF4. RNF4

35   deficiency also resulted in an accumulation of hyper-SUMOylated proteins in chromatin, including

36   members of the SMC5/6 complex, which contributes to replication failure by a mechanism

37   dependent on RAD51. These findings indicate that RNF4, which shows increased expression in

38   multiple human tumor types, is a potential target for anti-cancer therapy, especially in tumors

39   expressing c-*myc.*

40

41

Introduction

Healthy cell growth requires post-translational modification of proteins by addition of ubiquitin (Ub) or the Small Ubiquitin-like Modifier (SUMO) (1, 2). Ubiquitination and SUMOylation regulate almost every aspect of cellular physiology by modifying the function and stability of cellular proteins. DNA replication and repair are examples of the importance of SUMOylation and ubiquitination, which act in coordination to ensure productive outcomes in each case (3, 4).

In mammalian cells, RNF4 (RING Finger Protein 4), is a key SUMO-targeted E3 ubiquitin ligase (STUbL), which has a central importance in linking protein regulation by SUMOylation and ubiquitination. RNF4 contains four SUMO-Interacting Motifs (SIMs), which target the protein to SUMOylated substrates. The E3 ubiquitin ligase activity of homodimeric RNF4 subsequently transfers Ub from one of a number of different E2 conjugating enzymes to the substrate (5). RNF4 is known to target the PML:RARA fusion protein that is frequently found in acute promyelocytic leukemia (APL) (6). In response to arsenic trioxide treatment, PML undergoes increased SUMOylation, making it an improved target for RNF4 STUbL activity, leading to degradation of the PML-RARA fusion protein and successful treatment outcomes even without use of conventional cytotoxic chemotherapy (7).

In addition to regulation of PML stability, RNF4 is implicated in a range of cellular processes. Several studies, using siRNA knockdown, mutant cell lines, or DT40 cells, reported defects in the cellular response to DNA damage after loss of RNF4 activity (8-12). In particular, efficiency of the homologous recombination (HR) pathway was reported to be reduced in si*RNF4* cells, as a

65   consequence of a failure to load RPA and RAD51 at resected DNA double-strand breaks (13,

66   14). RNF4 also promotes normal chromosome segregation, based on its ability to remove toxic

67   DNA-protein crosslinks that interfere with mitosis (15). Mutations affecting other components of

68   the HR machinery, such as *BRCA1* or *BRCA2*, increase the rate of genetic mutations, leading to

69   substantially increased tumor risk (16). Around 6% of primary cancer cases are estimated to be

70   affected by HR deficiency (17), and identifying these cases is of substantial importance for

71   treatment, because HR-deficient cancers show greatly increased sensitivity to Poly(ADP-Ribose)

72   Polymerase (PARP) inhibitors and platinum-based cross-linking agents (18). Human *RNF4*

73   mutations that might predispose affected individuals to cancer have not yet been reported,

74   however, and the importance of *RNF4* as a tumor suppressor is unknown.

75

76   A challenge to evaluating the importance of RNF4 as a tumor suppressor is the lack of suitable

77   animal models to test whether loss of RNF4 increases the risk of malignant cell growth.

78   Homozygous deletion of the mouse *Rnf4* gene causes embryonic lethality prior to E15 (19). We

79   now report the use of a conditional-knockout *Rnf4* mouse model to test the importance of *Rnf4*

80   for DNA repair, and to evaluate how *Rnf4* deficiency contributes to tumor susceptibility. We find

81   that deletion of *Rnf4* causes genomic instability and reduced cellular viability. These phenotypes

82   of *Rnf4* deficiency are an outcome of defective DNA replication, and can be partially rescued by

83   inhibiting the ubiquitin isopeptidase, USP7. The increased genomic instability of *Rnf4*-deficient

84   cells does not lead to a higher frequency of malignant neoplasms, however, even on a p53-

85   deficient background. *Rnf4* deficiency instead significantly delayed the rate of tumor formation

86   in a mouse model of c-*myc* overexpression, indicating that *Rnf4* contributes to the growth of

87   incipient tumors. These results demonstrate that RNF4 is an essential factor for DNA replication

88   and a potential novel target for anti-cancer therapy.

89

90

91   Results

92

93   *Rnf4 deletion causes genomic instability and cell death in primary B cells*

94

95   To test the importance of RNF4 for growth of somatic cells, we first attempted to rescue

96   embryonic lethality in $Rnf4^{-/-}$ mice by crossing to $Trp53^{-/-}$ or $Trp53bp1^{-/-}$ mouse lines. Co-

97   deletion of p53 or 53BP1 in these lines rescues embryonic lethality in $Brca1^{\Delta11/\Delta11}$ mice [20], but

98   we were not able to obtain any viable $Rnf4^{-/-}$ pups by this approach, indicating that $Rnf4$ has an

99   indispensable role in normal embryonic development (Supplemental Table 1). We therefore

100   generated a novel, conditional $Rnf4^{fl}$ allele by introducing LoxP sites around $Rnf4$ exon 6 (Figure

101   1A). $Rnf4^{fl/fl}$ mice were crossed to *CD19-Cre* animals to delete $Rnf4$ selectively in the B

102   lymphocyte lineage [21]. The spleens of these $Rnf4$ conditional-knockout ($Rnf4^{\Delta/\Delta}$) mice showed

103   a near-normal population of mature B220$^+$ B cells, but RNF4 was undetectable in protein lysates

104   from these cells (Figure 1B and C). $Rnf4^{\Delta/\Delta}$ B cells showed a substantially increased proportion

105   of high-molecular-weight SUMOylated species, consistent with the known role of RNF4 in

106   ensuring turnover of SUMOylated proteins [6].

107

108   B cells lacking RNF4 showed clear signs of cell stress after 48 hrs of in vitro culture, with

109   stabilization of p53, and increased cleavage of caspase-3 (Figure 1C). Phosphorylation of KAP1,

110   and H2AX was also increased (Figure 1D), indicating activation of ATM and ATR after DNA

111   damage [22]. Markers of DNA damage and apoptosis became increasingly apparent after three

112   days of in vitro B cell culture, indicating an underlying stress that became more acute after a

113   longer period of B cell activation. Analysis of metaphase chromosomes revealed a significant

114 increase in chromosome aberrations in *Rnf4*$^{\Delta/\Delta}$ B cells (Figure 1E). This increase was apparent

115 after 24 hrs of in vitro culture, and reached an even greater level after 48 hrs of culture. There

116 was additionally an increase in the frequency of sister chromatid exchanges in *Rnf4*$^{\Delta/\Delta}$ cells,

117 indicating increased use of HR-mediated DNA repair (Supplemental Figure 1A). *Rnf4*$^{\Delta/\Delta}$ B cells

118 also showed a disrupted cell cycle, with a slightly reduced proportion of S phase cells, and an

119 increase in the proportion of cells in G2 phase (Figure 1F).

120

121 Consistent with the increased induction of apoptotic markers, the majority of *Rnf4*$^{\Delta/\Delta}$ B cells

122 became non-viable after three days in culture (Figure 1G). Cell death and increased genomic

123 instability was only observed in homozygous *Rnf4*$^{\Delta/\Delta}$ cells, and not in heterozygotes (Figure 1H

124 and I). Although p53 is clearly stabilized in *Rnf4*$^{\Delta/\Delta}$ cells (Figure 1C), deletion of *Trp53* only

125 partially rescued cell viability and had no significant impact on chromosome instability

126 (Supplemental Figure 1 B and C). RNF4 therefore plays an essential role for ensuring the

127 viability of proliferating primary B cells, and in its absence, cells undergo apoptosis by a

128 combination of p53-mediated and p53-independent processes.

129

130 *Rnf4-knockout cells show defects in DNA replication*

131

132 To evaluate the importance of RNF4 for DNA repair, we challenged *Rnf4*$^{\Delta/\Delta}$ cells with a range of

133 compounds that cause DNA damage of various kinds (Supplemental Figure 2A). These agents

134 included olaparib, a PARP inhibitor that produces DNA double-strand breaks in replicating cells;

135 ionizing radiation (IR), which produces DNA double-strand breaks in all phases of the cell cycle;

136 the DNA crosslinking agents, mitomycin C (MMC), and cisplatin (CDDP); and methyl

137   methanesulfonate (MMS), a DNA alkylating agent. In each case, $Rnf4^{\Delta/\Delta}$ cells showed an

138   increase in chromosome instability after treatment, but the increase in $Rnf4^{\Delta/\Delta}$ cells was not

139   significantly greater than that observed in WT cells after subtracting the rate of chromosome

140   breaks and rearrangements in the untreated condition (Supplemental Figure 2B). A high

141   frequency of chromosome aberrations was observed after olaparib or cisplatin treatment of

142    $Brca1^{\Delta11/\Delta11}$ cells, which express a hypomorphic form of BRCA1, and are HR-deficient (23)

143   (Figure 2A). In contrast, $Rnf4^{\Delta/\Delta}$ cells showed only a very mild increase in the frequency of

144   chromosome breaks and rearrangements after treatment with olaparib or cisplatin, despite having

145   a higher rate of chromosome instability in the absence of drug treatment. The relatively mild

146   sensitivity of $Rnf4^{\Delta/\Delta}$ cells after treatments to induce DNA damage suggests that defects in

147   additional cellular processes may contribute to the genomic instability and poor growth of these

148   cells.

149

150   The proliferation and viability of $Rnf4^{\Delta/\Delta}$ cells was significantly impacted by treatment with

151   either MMS, or the DNA polymerase inhibitor, aphidicolin (APH) (Figure 2B, and Supplemental

152   Figure 2C and D). These agents also induced strong caspase-3 cleavage in $Rnf4^{\Delta/\Delta}$ cells (Figure

153   2C). MMS produces cytotoxicity through production of single-stranded DNA breaks and by

154   inhibition of DNA replication (24-26). Although we did not detect an increase in single-strand

155   breaks in $Rnf4^{\Delta/\Delta}$ cells (Supplemental Figure 2E), we observed that $Rnf4^{\Delta/\Delta}$ cells were

156   hypersensitive to the replication inhibitors hydroxyurea, aphidicolin, and gemcitabine (Figure

157   2D). $Rnf4^{\Delta/\Delta}$ cells also showed an increase in 53BP1 G1 nuclear bodies, a hallmark of cells that

158   are encountering problems with DNA replication (Figure 2E) (27, 28). $Rnf4^{\Delta/\Delta}$ cells consistently

159   incorporated lower levels of the deoxythymidine analog, EdU, indicating a lower rate of DNA

160   replication (Figure 2F). To directly measure the activity of individual replication forks, we

161   performed a DNA combing analysis after pulsing cells with CldU and IdU, which revealed that

162   *Rnf4$^{\Delta/\Delta}$* cells showed a significant reduction in replication fork velocity (Figure 2G). *Rnf4$^{\Delta/\Delta}$* cells

163   also showed reduced stability of newly-replicated DNA after hydroxyurea treatment (Figure 2H).

164   ATR-mediated CHK1 phosphorylation is essential for signaling the presence of replication stress

165   (29), but phosphorylation of CHK1 was defective after induction of replication stress in the

166   absence of RNF4 (Figure 2I). Although replication forks in *Rnf4$^{\Delta/\Delta}$* cells appeared to restart

167   normally after HU treatment (Supplemental Figure 2F), and showed only marginal levels of fork

168   asymmetry (Supplemental Figure 2G), the reduction in replication fork progression induced by

169   MMS treatment in WT cells is not observed in RNF4-conditional-knockout cells (Supplemental

170   Figure 2H). A failure to adequately signal replication stress therefore correlates with reduced

171   replication efficiency in *Rnf4$^{\Delta/\Delta}$* cells.

172

173   *Replication defects and cell death in Rnf4$^{\Delta/\Delta}$ cells are a consequence of deregulated*

174   *SUMOylation*

175

176   Transduction of *Rnf4$^{\Delta/\Delta}$* B cells with a construct expressing WT RNF4 resulted in a rescue of cell

177   viability and EdU uptake (Fig 3A-B). This effect was not seen with RNF4 constructs containing

178   mutations in the E3 ubiquitin ligase active site, or in the SUMO-interaction motifs. The STUbL

179   activity of RNF4 is therefore essential for normal cell viability. To test whether the defective

180   DNA replication, genomic instability, and cell death observed in *Rnf4$^{\Delta/\Delta}$* cells are specifically

181   caused by the accumulation of high-MW SUMOylated proteins, we used inhibitors of Ubiquitin

182   Specific Protease 7 (USP7), a ubiquitin isopeptidase that removes ubiquitin from SUMOylated

183   substrates (30). Short-term treatment with USP7 inhibitor produced an increase in the amount of

184   ubiquitination of SUMOylated proteins (Supplemental Figure 3), indicating that other cellular E3

185   ubiquitin ligases target SUMOylated proteins at some level in the absence of RNF4. Continuous

186   treatment with the USP7 inhibitors, P22077 or P5091, substantially reversed the accumulation of

187   SUMOylated proteins in $Rnf4^{\Delta/\Delta}$ cells, presumably by stabilizing ubiquitin chains on those

188   proteins to enable proteasomal targeting (Figure 3C). This reduction in the quantity of

189   SUMOylated proteins was associated with a rescue in the speed of replication forks in $Rnf4^{\Delta/\Delta}$

190   cells (Figure 3D), reduced cell death (Figure 3E and F), and a reduction in the frequency of

191   chromosome aberrations (Figure 3G and H). These results suggest that the slow replication forks,

192   genomic instability, and increased cell death observed in $Rnf4^{\Delta/\Delta}$ cells arise because of a failure

193   to properly degrade SUMOylated proteins. Inhibition of SUMOylation by 2-D08, which blocks

194   transfer of SUMO from UBC9 to potential substrates (31), or by ML-792, which inhibits the

195   SUMO-Activating enzyme, SAE1/2 (32), also produced a partial rescue of chromosome

196   instability and cell death in $Rnf4^{\Delta/\Delta}$ cells (Figure 3I and J), showing that accumulation of poly-

197   SUMOylated proteins in $Rnf4^{\Delta/\Delta}$ cells is causative of reduced cell viability.

198

199   *Rnf4 deletion leads to defective recruitment of proteins required for replication stress responses*

200

201   To identify changes in cellular protein expression that might account for the genomic instability

202   and reduced viability of $Rnf4^{\Delta/\Delta}$ cells, we performed quantitative isobaric labeling mass

203   spectrometry with resting B cells (Day 0) and cells that were stimulated to divide in vitro for 48

204   hrs (Day 2). In resting B cells, there was no substantial difference in protein expression between

205   WT and $Rnf4^{\Delta/\Delta}$ cells (Figure 4A, Supplemental Table 2). After activation of B cells and the

206   initiation of cell division, there were substantial changes in protein abundance in both the WT

207   and *Rnf4*$^{\Delta/\Delta}$ samples (Figure 4B). Activated *Rnf4*$^{\Delta/\Delta}$ B cells showed a modest, but statistically-

208   significant increase in the abundance of 455 proteins encompassing a broad range of protein

209   classes (Supplemental Table 3, Supplemental Figure 4A and B). Increases in the abundance of

210   several of these proteins were validated by Western blotting (Figure 4C). The broad changes in

211   protein expression in *Rnf4*$^{\Delta/\Delta}$ B cells are consistent with previous proteomic studies, which

212   revealed that RNF4 targets a wide range of substrates (33, 34).

213

214   As *Rnf4*$^{\Delta/\Delta}$ cells appear to have specific problems with DNA replication, we next used iPOND

215   (isolation of Proteins On Nascent DNA) (35) to identify proteins with altered abundance at

216   replication forks (Supplemental Table 4). Protein enrichment analysis on candidate proteins that

217   showed substantially altered abundance at replication forks in *Rnf4*$^{\Delta/\Delta}$ cells revealed a cluster of

218   proteins around FANCD2 (Supplemental Figure 4C), including Fanconi Anemia family proteins

219   with known functions in ensuring stable replication (36). Several of these proteins show reduced

220   abundance at replication forks in *Rnf4*$^{\Delta/\Delta}$ cells (Figure 4D), potentially accounting for the

221   reduced replication efficiency seen in the absence of RNF4. The helicases PIF1 and RECQL5,

222   which are required for DNA replication through difficult substrates (37, 38), also show

223   diminished abundance in iPOND samples from RNF4-deficient cells. These results demonstrate

224   that *Rnf4*$^{\Delta/\Delta}$ cells show a deficiency in recruitment of proteins necessary for replication fork

225   stability and progression.

226

227   *Rnf4*$^{\Delta/\Delta}$ cells accumulate poly-SUMOylated proteins in chromatin (Supplemental Figure 4D). We

228   performed immunoprecipitation of SUMO2/3 on chromatin samples from WT and *Rnf4*$^{\Delta/\Delta}$ cells,

229   to attempt to identify hyper-SUMOylated chromatin proteins in $Rnf4^{\Delta/\Delta}$ samples, which might

230   contribute to defective replication fork progression. Mass spectrometry revealed a set of proteins

231   with two clusters including proteins involved in regulation of SUMOylation, which are known

232   targets of RNF4 (34), and several members of the SMC5/6 complex (Supplemental Table 5,

233   Supplemental Figure 4E and F). The SMC5/6 complex is regulated by SUMOylation, and

234   contributes to replication fork stability and regulation of recombination (39). SUMOylated

235   SMC5 and SMC6 were significantly enriched in chromatin from $Rnf4^{\Delta/\Delta}$ cells relative to WT

236   (Figure 4E). Three Non-SMC Element (NSMCE) subunits of the SMC5/6 complex were

237   additionally present at increased abundance in SUMO2/3 immunoprecipitated proteins (Figure

238   4F). The SMC5/6 complex therefore shows significant deregulation and hyper-SUMOylation in

239   chromatin of $Rnf4^{\Delta/\Delta}$ cells, which may contribute to deficiencies in responding to replication

240   stress.

241

242   *Cell death and genomic instability in RNF4-deficient cells are dependent on RAD51*

243

244   The SMC5/6 complex is known to prevent the accumulation of toxic recombination

245   intermediates that appear at stalled replication forks (39, 40). We observed that knockdown of

246   *RNF4* using multiple different siRNAs in U2OS EJ-DR reporter cells caused an increase in the

247   rate of HR-mediated repair of DNA double-strand breaks (Supplemental Figure 5A). Ionizing

248   radiation-induced foci of RAD51 formed normally in the nuclei of $Rnf4^{\Delta/\Delta}$ B cells (Supplemental

249   Figure 5B). To test whether a potential increase in DNA recombination in RNF4-deficient cells

250   might contribute to apoptosis and defective replication, we used the RAD51 inhibitors, RI-1 and

251   B02 (41, 42). At high concentrations, these agents can block formation of ionizing-radiation

12

252   induced RAD51 foci, and reduce HR efficiency in reporter assays (Supplemental Figure 5C and

253   D). Treatment with lower doses did not have a measurable impact on the cell cycle of WT cells

254   (Supplemental Figure 5E), but substantially improved the growth of RNF4-deficient B cells (Fig

255   5A-H). RAD51 inhibition significantly reduced the p53 activation and caspase-3 cleavage

256   normally observed in $Rnf4^{\Delta/\Delta}$ cells, reduced the frequency of chromosome aberrations, and

257   improved cell proliferation and viability. Improved growth of $Rnf4^{\Delta/\Delta}$ cells after RAD51

258   inhibition was associated with a rescue of replication fork velocity (Figure 5I). RAD51 did not

259   show an increased abundance at replication forks in iPOND data sets from $Rnf4^{\Delta/\Delta}$ cells,

260   however, nor is the overall abundance or level of ubiquitination of RAD51 substantially changed

261   (Supplemental Figure 5F-H). RAD51-mediated toxicity may arise because of dysregulation of

262   some other RNF4 target, as USP7 inhibition also reduced the hyper-recombinogenic phenotype

263   of siRNF4-treated cells (Supplemental Figure 5I). Targeting other proteins involved in

264   homologous recombination did not achieve a similar rescue of the phenotypes of RNF4

265   deficiency as was achieved with RAD51 inhibition. In particular, deletion of either *Brca1* or

266   *Brca2* did not result in an improvement in the proliferation, viability, or genomic integrity of

267    $Rnf4^{\Delta/\Delta}$ cells (Supplemental Figure 6A-F).

268

269   *Deletion of Rnf4 delays tumor formation in a c-myc cancer model*

270

271   As B cells from *Rnf4*-conditional-knockout mice showed substantial genomic instability (Figure

272   1E), we performed a longitudinal study to determine if *Rnf4*-conditional-knockout mice are at

273   increased risk of cancer. Despite elevated genomic instability in $Rnf4^{\Delta/\Delta}$ B cells grown in culture,

274   there was no difference in tumor susceptibility caused by deletion of *Rnf4* in the B cell lineage

275   (Figure 6A). The overall survival of conditional knockout and control mice also showed no

276   significant difference (Supplemental Figure 7A). Tumor susceptibility in *Brca1*- and *Brca2*-

277   deficient mice is more apparent in a p53-hemizygous background (43-45). We therefore crossed

278   *Rnf4*-conditional-knockout mice to a $Trp53^{+/-}$ background, to test whether loss of RNF4 causes

279   tumor outgrowth in cells lacking normal expression of p53. We observed that *Rnf4* deficiency

280   did not accelerate tumor formation, even on a $Trp53^{+/-}$ background (Figure 6B), or affect the

281   overall survival rate of $Trp53^{+/-}$ mice (Supplemental Figure 7B). As in the control group,

282    $Rnf4^{\Delta/\Delta};Trp53^{+/-}$ animals developed tumors characteristic of p53 loss-of-function, with a large

283   proportion of thymomas (46). Finally, we tested whether *Rnf4* deficiency causes accelerated

284   tumor formation in Eμ-*myc* mice, a transgenic model for overexpression of the oncogene, c-*myc*,

285   in B cells (47). As expected, mice carrying the Eμ-*myc* transgene had a very high incidence of B

286   cell lymphoma with a median survival rate of 123 days (Figure 6C). In contrast, mice expressing

287   Eμ-*myc* with conditional deletion of *Rnf4* in the B cell lineage showed a significant delay in

288   tumor formation, with a median tumor-free survival of 215 days. The overall lifespan of Eμ-

289   *myc;Rnf4*$^{\Delta/\Delta}$ mice showed an equivalent extension (Supplemental Figure 7C). These studies show

290   that *Rnf4* deletion does not predispose mice to tumor formation, and loss of *Rnf4* delays the onset

291   of tumors in cells with c-*myc* overexpression.

292

293   We considered whether defects in DNA replication might limit the growth of incipient *myc*-

294   dependent malignancies in mice carrying the Eμ-*myc* transgene. Consistent with the well-known

295   ability of c-*myc* to induce cellular proliferation, we observed EdU uptake by freshly-isolated Eμ-

296   *myc;Rnf4*$^{+/+}$ and Eμ-*myc;Rnf4*$^{\Delta/\Delta}$ B cells, whereas WT and $Rnf4^{\Delta/\Delta}$ B cells showed almost no EdU

297   incorporation (Supplemental Figure 7D). A proportion of Eμ-*myc* splenic B cells are therefore

14

298   dividing, even in the absence of any exogenous mitogenic stimulus. As was the case in $Rnf4^{\Delta/\Delta}$

299   cells, we measured an increased frequency of chromosome aberrations in Eμ-myc;$Rnf4^{\Delta/\Delta}$ B cells

300   relative to Eμ-myc;$Rnf4^{+/+}$ cells (Fig 6D). Eμ-myc;$Rnf4^{\Delta/\Delta}$ B cells also showed a significantly

301   reduced ability to proliferate in culture as compared to Eμ-myc;$Rnf4^{+/+}$ cells (Figure 6E). We

302   tested the effect of knocking down RNF4 on the growth of U2OS cells with a stably-integrated,

303   doxycycline-inducible c-myc construct (48). After knockdown of $RNF4$, these U2OS-iMYC cells

304   showed significantly reduced proliferation compared to cells transfected with control siRNA

305   (Figure 6F). In Eμ-myc-transgenic cells, deletion of $Rnf4$ also led to reduced replication fork

306   velocity, higher levels of γ-H2AX in S phase, and an increased number of 53BP1 G1 nuclear

307   bodies (Figure 6G and H, and Supplemental Figure 7E). These results are consistent with the

308   concept that the increased propensity of myc-transgenic cells to proliferate makes them acutely

309   sensitive to loss of RNF4, which is required for normal DNA replication.

310   To consider whether $RNF4$ expression might impact the growth of tumors in humans, we

311   analyzed survival of B cell acute lymphoblastic leukemia patients studied as part of the NCI

312   TARGET Phase II initiative. Patients with tumors expressing high levels of $RNF4$ had

313   significantly worse survival outcomes than those expressing normal levels of $RNF4$ (Fig 6I).

314   Elevated $RNF4$ expression is a feature of several tumor types in TCGA data sets (Supplemental

315   Figure 7F), and high $RNF4$ expression correlates with poor survival in multiple tumor types,

316   including breast adenocarcinoma, and lung adenocarcinoma (Supplemental Figure 7G-H). These

317   findings suggest that RNF4 may have a general role in supporting tumor outgrowth, by

318   facilitating DNA replication in malignant cells.

319

320 Discussion

321

322 Our observation that deletion of *Rnf4* does not lead to malignancy in B lymphocytes, even in the

323 absence of p53, is potentially surprising considering the high rate of genomic instability observed

324 in RNF4-deficient cells. Mice with deletions in known DNA repair genes, such as *Brca1* or

325 *Brca2*, show tumor susceptibility, especially on a p53-deficient background (43, 45). The rate of

326 chromosome instability in untreated *Rnf4*$^{\Delta/\Delta}$ B cells is significantly higher than that in

327 *Brca1*$^{\Delta 11/\Delta 11}$ B cells (Fig 2A), and yet no tumor susceptibility was observed in *Rnf4* conditional-

328 knockout mice. This outcome is potentially similar to the situation with cells lacking RAD51, the

329 central mediator of HR (49). Repression of *RAD51* expression leads to accumulation of

330 chromatid and chromosome breaks (50), but *RAD51* mutations do not correlate strongly with

331 cancer incidence (51). Mouse knockout studies have shown that loss of RAD51 causes a

332 complete block in cellular proliferation (52, 53), therefore it is likely that cancer cells cannot

333 survive in the absence of RAD51. Based on our results, we propose that a similar effect is caused

334 by loss of RNF4, in that knockout cells show chromosome instability, but are also unable to

335 replicate and divide normally, leading to cell death instead of malignancy.

336

337 We find that the block on cell growth caused by conditional inactivation of *Rnf4* is so strong as

338 to limit the outgrowth of c-*myc* dependent lymphomas. Tumors driven by *myc* activity are

339 dependent on SUMOylation, and SUMO regulators are upregulated by *myc* overexpression (54).

340 Our work further underscores the importance of SUMO regulation for tumor cell growth, and

341 reveals the importance of RNF4 in this pathway. The dependence of incipient tumor cells from

342 E*μ-myc* mice on RNF4 for survival and tumor outgrowth is an example of 'non-oncogene

16

343 addiction' (55). Increased proliferative signaling arising from *myc* overexpression leads to rapid

344 DNA replication, which can only be sustained if RNF4 is available to ensure appropriate

345 ubiquitination in replicating chromatin domains. A similar effect is seen with loss of ATR and

346 CHK1, which signal the presence of DNA replication stress, including that induced by oncogene

347 expression (29). CHK1 inhibition compromises the growth of tumors overexpressing oncogenic

348 Ras or Myc, and tumor formation is significantly reduced in Eμ-*myc* mice expressing mutant

349 ATR (56, 57).

350

351 Several studies in mammalian cells have supported a role for RNF4 in regulation of DNA

352 replication. In ATR-deficient cells, RNF4 promotes SLX4-mediated cleavage of replication

353 forks, leading to fork collapse and the appearance of DNA double-strand breaks (58). RNF4

354 knockdown also reduces the ability of replication forks to restart after persistent replication

355 stress, based on the ability of RNF4 to ubiquitinate BLM helicase (59). Another recent study

356 identified RNF4 as the factor responsible for removal of the ZAPP-TOP2a-PICH complex from

357 replication forks (33, 60). This finding is consistent with earlier studies, which showed that

358 RNF4 targets trapped TOP1- and TOP2-cleavage complexes for proteasomal degradation (61,

359 62). Several studies have identified PARP1 as a target of the E3 ubiquitin ligase activity of

360 RNF4 (63, 64). PARP1 is active at replication forks, and the cytotoxic effect of PARP inhibitors

361 is partially dependent on their ability to trap PARP1 on chromatin, creating a barrier to

362 replication fork progression (65). Although we observed modest increases in the abundance of

363 PARP1, TOP2A, and TOP2B in whole cell extracts from *Rnf4*$^{\Delta/\Delta}$ cells (Figure 4B and C), we did

364 not observe significant changes in these factors in iPOND-MS studies of proteins at active

365 replication forks. We did find reductions in the abundance of FANCD2, FANCI, and FANCM at

366   replication forks in RNF4-deficient cells (Fig 4D). Each of these factors is known to function in

367   ensuring replication fork progression and stability (66-68). The helicases PIF1 and RECQL5,

368   which are required for replication through challenging substrates such as G quadruplexes and

369   transcription-replication conflict sites, are also present at reduced abundance at replication forks

370   of $Rnf4^{\Delta/\Delta}$ cells (37, 38).

371

372   Work from the Fernandez-Capetillo lab has supported a model in which chromatin around active

373   DNA replication forks is marked by high levels of SUMOylation and low levels of ubiquitination

374   (69). According to this model, chromatin outside of active replicating regions is marked by lower

375   levels of SUMOylation, and high levels of ubiquitination. Disruption of the normal balance of

376   ubiquitin- and SUMO-conjugated proteins in replicating chromatin domains leads to a reduction

377   in replication fork progression (30). We find that SUMOylation is broadly increased in

378   chromatin in $Rnf4^{\Delta/\Delta}$ cells (Supplemental Figure 4D) and this increase correlates with reduced

379   replication fork velocity and cell survival. In particular, we identified five out of eight

380   components of the mammalian SMC5/6 complex as hyper-SUMOylated chromatin constituents

381   in $Rnf4^{\Delta/\Delta}$ cells (Figure 4E and F). The SMC5/6 complex, like other SMC complexes, is a multi-

382   protein assembly that encircles DNA and facilitates loop extrusion (70). The SMC5/6 complex

383   facilitates DNA replication by helping to relieve chromosome-wide superhelical tension that

384   arises around active replisomes (71). This process involves the prevention of intertwining of

385   sister chromatid molecules behind the replication fork. Depletion of SMC5/6 in yeast causes a

386   block in replication at the ribosomal DNA array (39). The SMC5/6 complex furthermore

387   physically interacts with FANCI and FANCD2 in mammalian cells (72), therefore defects in the

388   regulation of SMC5/6 may account for the reduced accumulation of FANCI and FANCD2 at

389   replication forks in $Rnf4^{\Delta/\Delta}$ cells. The processivity of replication forks in budding yeast is

390   dependent on the SMC5/6 complex, which limits MPH1-mediated fork regression, and promotes

391   error-free bypass of DNA lesions (73, 74). The ability of SMC5 to promote lesion bypass is

392   dependent on SUMOylation, therefore it is an attractive candidate for regulation by RNF4.

393

394   Toxic recombination intermediates accumulate in cells with deficiencies in the SMC5/6 complex

395   (39, 40, 75). The cytotoxic effects of RNF4 deletion are notably rescued by RAD51 inhibitors,

396   indicating that RAD51-dependent recombination or fork regression is causative of cell death in

397   the absence of RNF4. It is possible that toxic RAD51-depenent structures arise because of a

398   failure to adequately regulate or localize the SMC5/6 complex in RNF4-deficient cells.

399   Mutations in *slx5*, the yeast homolog of RNF4, are known to produce gross chromosomal

400   rearrangements caused by aberrant recombination between homeologous sequences (76).

401   Although the importance and details of specific mechanisms for RNF4-dependent regulation of

402   DNA replication remain to be resolved, it is clear that RNF4 is required for efficient replication,

403   and may therefore represent an attractive target for cancer cases driven by *myc,* or other

404   oncogenes that drive rapid cellular proliferation.

405

406   Methods

407

408   *Sex as a biological variable*

409

410   Sex was not considered as a biological variable in this study.

411

412   *Generation of Rnf4 conditional knockout mice*

413

414   Cas9:sgRNA ribonucleoprotein complexes were prepared by incubating eSpCas9 (Millipore-

415   Sigma) with sgRNA and then adding single-stranded oligodeoxynucleotides, which contained

416   homology arms flanking LoxP sequences. This mixture was microinjected into C57BL/6J

417   embryos. The 5' LoxP sgRNA spacer sequence was CAATCACTTGCCTTATAAGA

418   (Millipore-Sigma) and the 5' LoxP oligo donor sequence was 5'-

419   CAAGATCTTAGGCAGGAAGATGGATGCCTTTGGTCAGACATGTTGGTTTTACTGAAA

420   ATCTCTGCCATTGTACCATGGGCTGAGCCTTCT**ATAACTTCGTATAGCATACATTA**

421   **TACGAAGTTAT**TATAAGGCAAGTGATTGGCCTCAGTGCCTGGACAGGACCTTCTGA

422   G-3' (LoxP in bold). For the 3' LoxP, the sgRNA spacer sequence was

423   TTGGGTTCAGCTGTCTGCTC and the 3' LoxP donor oligo sequence was 5'-

424   ACAAGTATCTTCCAAGCAGCTAGGTAGGCATATTTGGAATACAGGGTTGGGTTCAGC

425   TGTCTGa**ATAACTTCGTATAGCATACATTATACGAAGTTAT**CTCAGGATAGACCAA

426   TTGACAGACAGACAGGGCCATACATACTGACCAGGGTGTGCTTTTCGCT-3' (LoxP in

427   bold, sequence in lower case added to create XmnI restriction site for screening). Three founders

428   were determined to have both LoxP sites correctly inserted flanking *Rnf4* exon 6. A single line

429   used for the study was backcrossed four times to C56Bl/6.

430

431   *Cell culture*

432

433   Primary B cells were isolated from mouse spleen and activated for in vitro culture with

434   lipopolysaccharide and interleukin 4 as previously described (77). U2OS Dox-inducible Myc-

435   GFP (U2OS-iMyc) cells (48) were seeded in triplicate with or without 0.5 μg/ml doxycycline

436   treatment in a 24-well plate after siRNA transfection. Eight days after seeding, proliferation was

437   assayed using CellTiter-Glo® Luminescent Cell Viability assay (#G7572, Promega) according to

438   the manufacturer's instructions. PLAT-GP cells (Cell Biolabs) were cultured in DMEM

439   containing 10% fetal bovine serum and 0.5% Penicillin-Streptomycin. For the in vivo

440   SUMOylation assay, FLAG-Rad51 plasmid was transfected into siRNA-treated U2OS cells

441   using Lipofectamine 2000. Cells were processed 24 hr after transfection as described (78).

442

443   *Antibodies, chemicals and plasmids*

444

445   Custom anti-RNF4 antibody was generated as previously described (79). Commercial antibodies

446   used in this study include: SUMO2/3 (ab3742; Abcam), p53 (2524; CST), Cleaved caspase-3

447   (9661; CST), Tubulin (T8238, Sigma), KAP1-pS824 (A300-767A; Bethyl), CHK1-pS345 (2341;

448   CST), CHK1 (sc-8408; Santa Cruz), γ-H2AX (05-636; Millipore), γ-H2AX-Alexa 488 (20304S;

449   CST), Histone H3 (ab1791; Abcam), TOP2a (sc-365916; Santa Cruz), TOP2b (MAB6348;

450   Novus), PARP1 (9542; CST), RNF10 (16936-1-AP; Proteintech). Antibody specific for mouse

451   POLD4 was provided by Marietta Lee. The following chemicals were used: olaparib (S1060;

452   Selleckchem), hydroxyurea (H8627; Sigma Aldrich), aphidicolin (A4487; Sigma Aldrich),

453   cisplatin (S1166; Selleckchem), MMS (129925; Sigma Aldrich), gemcitabine (G6423; Sigma

454   Aldrich), P22077 (662142; Sigma Aldrich), P5091 (2277; Biovision), 2-D08 (SML1052; Sigma

455   Aldrich), ML-792 (407886, MedKoo), RI-1 (SML1294; Sigma Aldrich), B-02 (SML0364;

456   Sigma Aldrich). For plasmids, human *RAD51* cDNA was inserted into pRK5-FLAG and human

457   *RNF4* cDNA was inserted into pMX-PIE-IRES-eGFP. Amino acid substitutions for *RNF4*-CS

458   and *RNF4*-ΔSIM were performed as described (78, 80).

459

460   *Chromatin fractionation and immunoprecipitation*

461

462   For chromatin fractionation, harvested cells were gently resuspended in Buffer A (10 mM

463   HEPES [pH7.9], 1.5 mM $MgCl_2$, 10 mM KCl, 0.05% NP-40, 0.5 mM DTT, 10 mM NEM, 50

464   mM glycerol-2-phosphate, supplemented with protease-inhibitor cocktail, Roche) and incubated

465   for 10min on ice. Cell nuclei were collected by centrifugation (5 min, 1,300 x g, 4°C) and

466   incubated in Buffer B (3 mM EDTA, 0.2 mM EGTA, 0.5 mM DTT, 10 mM NEM, 50mM

467   glycerol-2-phosphate, and protease-inhibitor cocktail) for 30min. The chromatin component was

468   collected by centrifugation (4 min, 1,700 x g, 4°C) and lysed with Buffer C (20mM HEPES

469   [pH7.9], 500 mM NaCl, 1.5 mM $MgCl_2$, 0.2mM EDTA, 0.5 mM DTT, 125 U / ml benzonase, 10

470   mM NEM, 50 mM glycerol-2-phosphate, and protease-inhibitor cocktail). Lysates were

471   incubated for 5 min at 37°C on a shaking heat block followed by 20 min incubation on ice. After

472   centrifugation at 16,000 g for 20 min, supernatant containing chromatin-bound protein was

473   collected. Anti-SUMO2/3 immunoprecipitation of chromatin fractions was performed after 10-

474 fold dilution of chromatin samples in dilution buffer (50 mM Tris-HCl [pH 7.5], 150 mM NaCl,

475 0.5% NP-40, 10 mM NEM, 50mM glycerol-2-phosphate, and protease-inhibitor cocktail), with

476 protein G-Agarose used for collection.

477

478 *Double-strand break repair reporter assay*

479

480 The EJ-DR assay was performed as previously described (81). To induce incorporated I-Sce1,

481 Shield1 (632189; Clontech) and triamcinolone (T6510; Sigma Aldrich) ligands were added to the

482 media for 24 h. Where necessary, RAD51 inhibitors were added together with the Shield1 and

483 triamcinolone. NHEJ and HR repair activity was assessed by quantification of DsRed- and GFP-

484 positive cells on BD FACS Calibur system and analyzed on FlowJo (Tree Star) 48hrs after

485 induction.

486

487 *siRNA depletion*

488

489 Cells were transfected with siRNA using Lipofectamine RNAiMAX (13778; Invitrogen). The

490 following siRNA oligonucleotides were used in this study: MISSION siRNA Universal Negative

491 Control #1 (SIC001, Sigma-Aldrich), siGENOME Human RNF4 siRNA set of 4 (M-006557-03;

492 Dharmacon), siRNF4-1 (D-006557-03), siRNF4-2 (D-006557-04), siRNF4-3 (D-006557-05),

493 siRNF-UTR (GGGCAUGAAAGGUUGAGAA), siGENOME Human BRCA1 siRNA set of 4

494 (M-003461-02; Dharmacon), siGENOME Human BRCA2 siRNA set of 4 (M-003462-01;

495 Dharmacon).

496

497   *Flow cytometry*

498

499   For the CFSE proliferation assay, purified B cells were resuspended at 1x 10^7 cells/ml in RPMI

500   medium, labeled with 5 μM CFSE for 10 min at 37°C, then cultured in RPMI medium with or

501   without IL-4 and LPS for 72 h. The CFSE fluorescence of unstimulated cells was taken as 100%

502   and the number of additional cell divisions was calculated according to reduced CFSE

503   fluorescence as the cells divided. Number of cell divisions was calculated as $\log_2$(median

504   intensity of unstimulated cells / median intensity of indicated cells). For EdU incorporation, B

505   cells were pulsed with 30 μM EdU for 30 min, and fixed with ice-cold methanol for 20 min. EdU

506   was detected using the Click-iT EdU Alexa Fluor-647 imaging kit. Cells were stained with DAPI

507   to measure DNA content. For flow cytometry analysis of splenocyte populations, mouse

508   splenocytes were treated with ACK lysis buffer for 5 min, then blocked with anti-CD16/CD32

509   antibody for 10 min at room temperature and labeled with B220-A647 (557683; BD) and CD43-

510   PE (12-0431-82; Invitrogen) for 1 hr at 4°C. Cytometry was performed using a BD FACSCalibur

511   or Cytek Aurora with analysis in FlowJo.

512

513   *Alkaline Comet assay*

514

515   Alkaline comet assays were performed using CometAssay kit (Trevigen) according to the

516   manufacturer's protocol. Splenic B cells were cultured for 48 hrs in vitro and then treated with

517   mock or 100 μM MMS treatment for 3 hrs. Images were acquired by Nikon Eclipse E800

518   epifluorescence microscope and analyzed with OpenComet software.

519

520   *DNA combing and DNA fiber analysis*

521

522   To measure fork speed, cells were incubated with 20 μM 5-chlorodeoxyuridine (CldU; C6891;

523   Sigma-Aldrich) for 20 min, followed by 20 min of incubation with 100 μM 5-iododeoxyuridine

524   (IdU; I7125; Sigma-Aldrich). Genomic DNA purification and combing on glass coverslips was

525   performed using materials and a protocol from Genomic Vision. DNA fiber analysis was

526   performed as described (82). The DNA was stained with anti-CldU antibody (ab6326; Abcam)

527   and anti-IdU antibody (347580; BD) for 1 h, followed by incubation with secondary antibodies

528   for 45 min. Images were acquired by Nikon Eclipse E800 epifluorescence microscope using a

529   40x objective and analyzed with ImageJ software.

530

531   *iPOND*

532

533   iPOND was performed as previously described (35).

534

535   *Retroviral transduction*

536

537   To express the human *RNF4* gene in B cells, retroviral vectors were transfected into PLAT-GP

538   cells using Lipofectamine 2000. B cells were cultured for 36 hrs of in vitro culture and

539   spinoculated with retroviral supernatants at 1150 g for 1.5 hr in the presence of 10 μg/ml

540   polybrene. After 4 hr at 37°C, supernatants were replaced with normal medium. The percentage

541   of GFP$^+$ and DAPI$^-$ B cells was measured with flow cytometry on Day 2 and Day 3 to check the

542   infection rates and viability.

543

Preparation of metaphase spreads and FISH

545

Telomere DNA FISH analysis was performed and analyzed as previously described (77). Images

were acquired by an AxioImager.Z2 microscope (Zeiss) using a 60x objective with MetaSystems

automatic stage. At least 50 metaphases were analyzed for each experiment.

549

Mass spectrometry

551

Thirty micrograms of each sample were digested in-gel with trypsin (1:50 ratio, sequencing

grade, Thermo Scientific Cat#90058) and peptides extracted as described previously (83, 84).

Peptides were labeled with Thermo TMTpro 16 Plex (Lot #: WC320807) and prefractionated by

high-pH RPLC. Mass spectrometry was conducted using SPS-MS3 to measure reporter ion

intensities on an Orbitrap Eclipse Tribrid Mass Spectrometer (Thermo Fisher). Instrument

settings were for MS1: Orbitrap resolution 120,000, scan range from 350–1600 Th, automatic

gain control (AGC) target 1E6, maximum injection time 100 ms; for MS2, Top 5 (3 sec) duty

cycle, quadrupole ion trap, AGC 2E4, collision energy 35, maximum injection time 35 ms,

isolation window was set at 0.7; and for MS3, 10 MS2 fragment ions captured as MS3 precursors

using isolation waveforms with multiple frequency notches, Orbitrap AGC 1.5E5, maximum

injection time 54 ms in the higher-energy collisional dissociation (HCD) cell and fragmented

with HCD with collision energy of 55% and scanned in the Orbitrap with scan range 100-500

m/z. Peak lists were generated by Thermo Proteome Discoverer (v. 2.1) as MASCOT Generic

Format (MGF) files and combined MS2-MS3 peak lists searched against the Uniprot mouse

566   database using an in-house version of X!Tandem (GPM Fury) (85). TMT MS3 reporter ion

567   intensities were extracted with correction for isotope channel crossover using custom in-house

568   software and exported to Excel. For each protein, the sum of TMT MS3 intensities for all

569   corresponding peptides were first normalized to the sum of the TMT intensities for each channel

570   to account for differences in labeling efficiency or amount of protein labeled for each channel.

571   The mean of the four replicates for each genotype/time-point was used to generate ratios for

572   selected comparisons. Proteins were filtered for those with 2 or more assigned spectra. Proteins

573   showing an increase of >10% in $Rnf4^{\Delta/\Delta}$ cells relative to WT cells with a P value < 0.05 (t-test)

574   were considered for further analysis.

575

576   For data-independent acquisition, instrument settings were: MS scan range set to 400-1200 m/z,

577   with resolution 12,000, AGC 3E6 and ion time set as auto. Eight m/z windows were used to

578   sequentially isolate (AGC 4E5 and ion time auto) and fragment ions in the C-trap using a relative

579   collision energy of 30. MS/MS spectra were recorded with a resolution of 30,000. Data were

580   analyzed using DIA-NN 1.8.1 (86) with default settings for FASTA digest for library-free search

581   / library generation and deep learning-based spectra and retention time prediction using Uniprot

582   reference proteomes UP000000589 (mouse). Data were normalized using the MaxLFQ

583   algorithm (87) and total normalized precursor intensities for each protein group were filtered for

584   both PEP (an estimate of the posterior error probability for the precursor identification, based on

585   scoring with neural networks) filter <0.01 and PG.Q (Protein Group Q Value) filter <0.01. T-

586   tests were calculated as above.

587

588   *Statistics*

589

590   Statistical tests were performed as described. P < 0.05 was considered to be statistically

591   significant. Where shown, n.s. indicates not significant. * indicates a P value < 0.05. ** indicates

592   a P value < 0.01. *** indicates a P value < 0.001. **** indicates a P value < 0.0001. Data points

593   on graphs represent results from a minimum of n=3 biological replicates. For beeswarm plots,

594   small data points represent individual values from n=3 experiments, separately colored, and large

595   data points indicate the mean of each experiment.

596

597   *Analysis of genomic data sets*

598

599   Functional categorization and measurements of statistical over-representation of protein classes

600   was performed using PANTHER (panther.db). STRING analysis was performed using tools at

601   https://string-db.org. cBioPortal (https://www.cbioportal.org) was used to access data on 72

602   pediatric acute lymphoblastic leukemia patients studied as part of the Therapeutically Applicable

603   Research to Generate Effective Treatments initiative, phs000218 (TARGET Phase II). The data

604   used for this analysis are available at https://portal.gdc.cancer.gov/projects. Overall survival of

605   patients with tumors with high *RNF4* mRNA expression (RNASeq z-score vs RSEM ≥ 2.0) was

606   compared to patients with *RNF4* mRNA in the unaltered range. cBioPortal was additionally used

607   to retrieve data on survival of patients with above-median and below median *RNF4* expression in

608   tumor biopsies, based on samples from 1,082 breast adenocarcinoma patients and 501 lung

609   adenocarcinoma patients studied as part of the TCGA PanCancer Atlas project (88). Analysis of

610   RNF4 expression in multiple tumor types was based on TCGA data accessed with the University

611   of Alabama Cancer Data analysis portal (89)

612

613   *Study Approval*

614

615   Vertebrate animal studies were carried out under an animal protocol approved by the Rutgers

616   University Institutional Animal Care and Use Committee.

617

618   *Data availability*

619

620   Proteomic data sets were deposited to the MassIVE database with accession numbers

621   MSV000090142, MSV000093660 and MSV000093661. All data used for figures is available in

622   a Supporting Data Values file.

623

624

625   Author Contributions

626

627   Experiments were conceived by J.H. and S.F.B. and performed by JH, except mass spectrometry,

628   which was performed by H.Z. The paper was written by S.F.B.

629

641   References

642

643   1.   Rape M. Ubiquitylation at the crossroads of development and disease. *Nat Rev Mol Cell*
644   *Biol.* 2018;19(1):59-70.
645   2.   Vertegaal ACO. Signalling mechanisms and cellular functions of SUMO. *Nat Rev Mol*
646   *Cell Biol.* 2022.
647   3.   Garcia-Rodriguez N, Wong RP, and Ulrich HD. Functions of Ubiquitin and SUMO in
648   DNA Replication and Replication Stress. *Front Genet.* 2016;7:87.
649   4.   Jackson SP, and Durocher D. Regulation of DNA damage responses by ubiquitin and
650   SUMO. *Mol Cell.* 2013;49(5):795-807.
651   5.   DiBello A, Datta AB, Zhang X, and Wolberger C. Role of E2-RING Interactions in
652   Governing RNF4-Mediated Substrate Ubiquitination. *J Mol Biol.* 2016;428(23):4639-50.
653   6.   Tatham MH, Geoffroy MC, Shen L, Plechanovova A, Hattersley N, Jaffray EG, et al.
654   RNF4 is a poly-SUMO-specific E3 ubiquitin ligase required for arsenic-induced PML
655   degradation. *Nat Cell Biol.* 2008;10(5):538-46.
656   7.   Osman AEG, Anderson J, Churpek JE, Christ TN, Curran E, Godley LA, et al. Treatment
657   of Acute Promyelocytic Leukemia in Adults. *J Oncol Pract.* 2018;14(11):649-57.
658   8.   Guzzo CM, Berndsen CE, Zhu J, Gupta V, Datta A, Greenberg RA, et al. RNF4-
659   dependent hybrid SUMO-ubiquitin chains are signals for RAP80 and thereby mediate the
660   recruitment of BRCA1 to sites of DNA damage. *Sci Signal.* 2012;5(253):ra88.
661   9.   Hirota K, Tsuda M, Murai J, Takagi T, Keka IS, Narita T, et al. SUMO-targeted ubiquitin
662   ligase RNF4 plays a critical role in preventing chromosome loss. *Genes Cells.*
663   2014;19(10):743-54.
664   10.   Luo K, Deng M, Li Y, Wu C, Xu Z, Yuan J, and Lou Z. CDK-mediated RNF4
665   phosphorylation regulates homologous recombination in S-phase. *Nucleic Acids Res.*
666   2015;43(11):5465-75.
667   11.   Luo K, Zhang H, Wang L, Yuan J, and Lou Z. Sumoylation of MDC1 is important for
668   proper DNA damage response. *EMBO J.* 2012;31(13):3008-19.
669   12.   Xie J, Kim H, Moreau LA, Puhalla S, Garber J, Al Abo M, et al. RNF4-mediated
670   polyubiquitination regulates the Fanconi anemia/BRCA pathway. *J Clin Invest.*
671   2015;125(4):1523-32.
672   13.   Galanty Y, Belotserkovskaya R, Coates J, and Jackson SP. RNF4, a SUMO-targeted
673   ubiquitin E3 ligase, promotes DNA double-strand break repair. *Genes Dev.*
674   2012;26(11):1179-95.
675   14.   Yin Y, Seifert A, Chua JS, Maure JF, Golebiowski F, and Hay RT. SUMO-targeted
676   ubiquitin E3 ligase RNF4 is required for the response of human cells to DNA damage.
677   *Genes Dev.* 2012;26(11):1196-208.
678   15.   Liu JCY, Kuhbacher U, Larsen NB, Borgermann N, Garvanska DH, Hendriks IA, et al.
679   Mechanism and function of DNA replication-independent DNA-protein crosslink repair
680   via the SUMO-RNF4 pathway. *EMBO J.* 2021;40(18):e107413.
681   16.   Helleday T. Homologous recombination in cancer development, treatment and
682   development of drug resistance. *Carcinogenesis.* 2010;31(6):955-60.
683   17.   Nguyen L, J WMM, Van Hoeck A, and Cuppen E. Pan-cancer landscape of homologous
684   recombination deficiency. *Nat Commun.* 2020;11(1):5584.

685   18.   O'Kane GM, Connor AA, and Gallinger S. Characterization, Detection, and Treatment
686   Approaches for Homologous Recombination Deficiency in Cancer. *Trends Mol Med.*
687   2017;23(12):1121-37.
688   19.   Hu XV, Rodrigues TM, Tao H, Baker RK, Miraglia L, Orth AP, et al. Identification of
689   RING finger protein 4 (RNF4) as a modulator of DNA demethylation through a
690   functional genomics screen. *Proc Natl Acad Sci U S A.* 2010;107(34):15087-92.
691   20.   Cao L, Xu X, Bunting SF, Liu J, Wang RH, Cao LL, et al. A selective requirement for
692   53BP1 in the biological response to genomic instability induced by Brca1 deficiency.
693   *Mol Cell.* 2009;35(4):534-41.
694   21.   Rickert RC, Roes J, and Rajewsky K. B lymphocyte-specific, Cre-mediated mutagenesis
695   in mice. *Nucleic Acids Res.* 1997;25(6):1317-8.
696   22.   Marechal A, and Zou L. DNA damage sensing by the ATM and ATR kinases. *Cold*
697   *Spring Harb Perspect Biol.* 2013;5(9).
698   23.   Xu X, Wagner KU, Larson D, Weaver Z, Li C, Ried T, et al. Conditional mutation of
699   Brca1 in mammary epithelial cells results in blunted ductal morphogenesis and tumour
700   formation. *Nat Genet.* 1999;22(1):37-43.
701   24.   Groth P, Auslander S, Majumder MM, Schultz N, Johansson F, Petermann E, and
702   Helleday T. Methylated DNA causes a physical block to replication forks independently
703   of damage signalling, O(6)-methylguanine or DNA single-strand breaks and results in
704   DNA damage. *J Mol Biol.* 2010;402(1):70-82.
705   25.   Hashimoto Y, Ray Chaudhuri A, Lopes M, and Costanzo V. Rad51 protects nascent
706   DNA from Mre11-dependent degradation and promotes continuous DNA synthesis. *Nat*
707   *Struct Mol Biol.* 2010;17(11):1305-11.
708   26.   Soll JM, Sobol RW, and Mosammaparast N. Regulation of DNA Alkylation Damage
709   Repair: Lessons and Therapeutic Opportunities. *Trends Biochem Sci.* 2017;42(3):206-18.
710   27.   Harrigan JA, Belotserkovskaya R, Coates J, Dimitrova DS, Polo SE, Bradshaw CR, et al.
711   Replication stress induces 53BP1-containing OPT domains in G1 cells. *J Cell Biol.*
712   2011;193(1):97-108.
713   28.   Lukas C, Savic V, Bekker-Jensen S, Doil C, Neumann B, Pedersen RS, et al. 53BP1
714   nuclear bodies form around DNA lesions generated by mitotic transmission of
715   chromosomes under replication stress. *Nat Cell Biol.* 2011;13(3):243-53.
716   29.   Yazinski SA, and Zou L. Functions, Regulation, and Therapeutic Implications of the
717   ATR Checkpoint Pathway. *Annu Rev Genet.* 2016;50:155-73.
718   30.   Lecona E, Rodriguez-Acebes S, Specks J, Lopez-Contreras AJ, Ruppen I, Murga M, et
719   al. USP7 is a SUMO deubiquitinase essential for DNA replication. *Nat Struct Mol Biol.*
720   2016;23(4):270-7.
721   31.   Kim YS, Keyser SG, and Schneekloth JS, Jr. Synthesis of 2',3',4'-trihydroxyflavone (2-
722   D08), an inhibitor of protein sumoylation. *Bioorg Med Chem Lett.* 2014;24(4):1094-7.
723   32.   He X, Riceberg J, Soucy T, Koenig E, Minissale J, Gallery M, et al. Probing the roles of
724   SUMOylation in cancer cell biology by using a selective SAE inhibitor. *Nat Chem Biol.*
725   2017;13(11):1164-71.
726   33.   Ding L, Luo Y, Tian T, Chen X, Yang Y, Bu M, et al. RNF4 controls the extent of
727   replication fork reversal to preserve genome stability. *Nucleic Acids Res.*
728   2022;50(10):5672-87.

729   34.   Kumar R, Gonzalez-Prieto R, Xiao Z, Verlaan-de Vries M, and Vertegaal ACO. The
730   STUbL RNF4 regulates protein group SUMOylation by targeting the SUMO conjugation
731   machinery. *Nat Commun.* 2017;8(1):1809.

732   35.   Sirbu BM, McDonald WH, Dungrawala H, Badu-Nkansah A, Kavanaugh GM, Chen Y,
733   et al. Identification of proteins at active, stalled, and collapsed replication forks using
734   isolation of proteins on nascent DNA (iPOND) coupled with mass spectrometry. *J Biol*
735   *Chem.* 2013;288(44):31458-67.

736   36.   Niraj J, Farkkila A, and D'Andrea AD. The Fanconi Anemia Pathway in Cancer. *Annu*
737   *Rev Cancer Biol.* 2019;3:457-78.

738   37.   Byrd AK, and Raney KD. Structure and function of Pif1 helicase. *Biochem Soc Trans.*
739   2017;45(5):1159-71.

740   38.   Urban V, Dobrovolna J, Huhn D, Fryzelkova J, Bartek J, and Janscak P. RECQ5 helicase
741   promotes resolution of conflicts between replication and transcription in human cells. *J*
742   *Cell Biol.* 2016;214(4):401-15.

743   39.   Peng XP, and Zhao X. The multi-functional Smc5/6 complex in genome protection and
744   disease. *Nat Struct Mol Biol.* 2023;30(6):724-34.

745   40.   Menolfi D, Delamarre A, Lengronne A, Pasero P, and Branzei D. Essential Roles of the
746   Smc5/6 Complex in Replication through Natural Pausing Sites and Endogenous DNA
747   Damage Tolerance. *Mol Cell.* 2015;60(6):835-46.

748   41.   Budke B, Logan HL, Kalin JH, Zelivianskaia AS, Cameron McGuire W, Miller LL, et al.
749   RI-1: a chemical inhibitor of RAD51 that disrupts homologous recombination in human
750   cells. *Nucleic Acids Res.* 2012;40(15):7347-57.

751   42.   Huang F, and Mazin AV. A small molecule inhibitor of human RAD51 potentiates breast
752   cancer cell killing by therapeutic agents in mouse xenografts. *PLoS One.*
753   2014;9(6):e100993.

754   43.   Jonkers J, Meuwissen R, van der Gulden H, Peterse H, van der Valk M, and Berns A.
755   Synergistic tumor suppressor activity of BRCA2 and p53 in a conditional mouse model
756   for breast cancer. *Nat Genet.* 2001;29(4):418-25.

757   44.   Liu X, Holstege H, van der Gulden H, Treur-Mulder M, Zevenhoven J, Velds A, et al.
758   Somatic loss of BRCA1 and p53 in mice induces mammary tumors with features of
759   human BRCA1-mutated basal-like breast cancer. *Proc Natl Acad Sci U S A.*
760   2007;104(29):12111-6.

761   45.   Xu X, Qiao W, Linke SP, Cao L, Li WM, Furth PA, et al. Genetic interactions between
762   tumor suppressors Brca1 and p53 in apoptosis, cell cycle and tumorigenesis. *Nat Genet.*
763   2001;28(3):266-71.

764   46.   Donehower LA, Harvey M, Slagle BL, McArthur MJ, Montgomery CA, Jr., Butel JS,
765   and Bradley A. Mice deficient for p53 are developmentally normal but susceptible to
766   spontaneous tumours. *Nature.* 1992;356(6366):215-21.

767   47.   Adams JM, Harris AW, Pinkert CA, Corcoran LM, Alexander WS, Cory S, et al. The c-
768   myc oncogene driven by immunoglobulin enhancers induces lymphoid malignancy in
769   transgenic mice. *Nature.* 1985;318(6046):533-8.

770   48.   Nie Z, Guo C, Das SK, Chow CC, Batchelor E, Simons SSJ, and Levens D. Dissecting
771   transcriptional amplification by MYC. *Elife.* 2020;9.

772   49.   Matos-Rodrigues G, Guirouilh-Barbat J, Martini E, and Lopez BS. Homologous
773   recombination, cancer and the 'RAD51 paradox'. *NAR Cancer.* 2021;3(2):zcab016.

774 50. Sonoda E, Sasaki MS, Buerstedde JM, Bezzubova O, Shinohara A, Ogawa H, et al.
775   Rad51-deficient vertebrate cells accumulate chromosomal breaks prior to cell death.
776   *EMBO J.* 1998;17(2):598-608.
777 51. Ameziane N, May P, Haitjema A, van de Vrugt HJ, van Rossum-Fikkert SE, Ristic D, et
778   al. A novel Fanconi anaemia subtype associated with a dominant-negative mutation in
779   RAD51. *Nat Commun.* 2015;6:8829.
780 52. Lim DS, and Hasty P. A mutation in mouse rad51 results in an early embryonic lethal
781   that is suppressed by a mutation in p53. *Mol Cell Biol.* 1996;16(12):7133-43.
782 53. Tsuzuki T, Fujii Y, Sakumi K, Tominaga Y, Nakao K, Sekiguchi M, et al. Targeted
783   disruption of the Rad51 gene leads to lethality in embryonic mice. *Proc Natl Acad Sci U
784   S A.* 1996;93(13):6236-40.
785 54. Hoellein A, Fallahi M, Schoeffmann S, Steidle S, Schaub FX, Rudelius M, et al. Myc-
786   induced SUMOylation is a therapeutic vulnerability for B-cell lymphoma. *Blood.*
787   2014;124(13):2081-90.
788 55. Luo J, Solimini NL, and Elledge SJ. Principles of cancer therapy: oncogene and non-
789   oncogene addiction. *Cell.* 2009;136(5):823-37.
790 56. Gilad O, Nabet BY, Ragland RL, Schoppy DW, Smith KD, Durham AC, and Brown EJ.
791   Combining ATR suppression with oncogenic Ras synergistically increases genomic
792   instability, causing synthetic lethality or tumorigenesis in a dosage-dependent manner.
793   *Cancer Res.* 2010;70(23):9693-702.
794 57. Murga M, Campaner S, Lopez-Contreras AJ, Toledo LI, Soria R, Montana MF, et al.
795   Exploiting oncogene-induced replicative stress for the selective killing of Myc-driven
796   tumors. *Nat Struct Mol Biol.* 2011;18(12):1331-5.
797 58. Ragland RL, Patel S, Rivard RS, Smith K, Peters AA, Bielinsky AK, and Brown EJ.
798   RNF4 and PLK1 are required for replication fork collapse in ATR-deficient cells. *Genes
799   Dev.* 2013;27(20):2259-73.
800 59. Ellis N, Zhu J, Yagle MK, Yang WC, Huang J, Kwako A, et al. RNF4 Regulates the
801   BLM Helicase in Recovery From Replication Fork Collapse. *Front Genet.*
802   2021;12:753535.
803 60. Tian T, Bu M, Chen X, Ding L, Yang Y, Han J, et al. The ZATT-TOP2A-PICH Axis
804   Drives Extensive Replication Fork Reversal to Promote Genome Stability. *Mol Cell.*
805   2021;81(1):198-211 e6.
806 61. Sciascia N, Wu W, Zong D, Sun Y, Wong N, John S, et al. Suppressing proteasome
807   mediated processing of topoisomerase II DNA-protein complexes preserves genome
808   integrity. *Elife.* 2020;9.
809 62. Sun Y, Miller Jenkins LM, Su YP, Nitiss KC, Nitiss JL, and Pommier Y. A conserved
810   SUMO pathway repairs topoisomerase DNA-protein cross-links by engaging ubiquitin-
811   mediated proteasomal degradation. *Sci Adv.* 2020;6(46).
812 63. Krastev DB, Li S, Sun Y, Wicks AJ, Hoslett G, Weekes D, et al. The ubiquitin-dependent
813   ATPase p97 removes cytotoxic trapped PARP1 from chromatin. *Nat Cell Biol.*
814   2022;24(1):62-73.
815 64. Martin N, Schwamborn K, Schreiber V, Werner A, Guillier C, Zhang XD, et al. PARP-1
816   transcriptional activity is regulated by sumoylation upon heat shock. *EMBO J.*
817   2009;28(22):3534-48.
818 65. Murai J, Huang SY, Das BB, Renaud A, Zhang Y, Doroshow JH, et al. Trapping of
819   PARP1 and PARP2 by Clinical PARP Inhibitors. *Cancer Res.* 2012;72(21):5588-99.

820   66.   Schlacher K, Wu H, and Jasin M. A distinct replication fork protection pathway connects
821   Fanconi anemia tumor suppressors to RAD51-BRCA1/2. *Cancer Cell.* 2012;22(1):106-
822   16.
823   67.   Schwab RA, Blackford AN, and Niedzwiedz W. ATR activation and replication fork
824   restart are defective in FANCM-deficient cells. *EMBO J.* 2010;29(4):806-18.
825   68.   Yang Y, Xu W, Gao F, Wen C, Zhao S, Yu Y, et al. Transcription-replication conflicts in
826   primordial germ cells necessitate the Fanconi anemia pathway to safeguard genome
827   stability. *Proc Natl Acad Sci U S A.* 2022;119(34):e2203208119.
828   69.   Lecona E, and Fernandez-Capetillo O. A SUMO and ubiquitin code coordinates protein
829   traffic at replication factories. *Bioessays.* 2016;38(12):1209-17.
830   70.   Pradhan B, Kanno T, Umeda Igarashi M, Loke MS, Baaske MD, Wong JSK, et al. The
831   Smc5/6 complex is a DNA loop-extruding motor. *Nature.* 2023;616(7958):843-8.
832   71.   Kegel A, Betts-Lindroos H, Kanno T, Jeppsson K, Strom L, Katou Y, et al. Chromosome
833   length influences replication-induced topological stress. *Nature.* 2011;471(7338):392-6.
834   72.   Rossi F, Helbling-Leclerc A, Kawasumi R, Jegadesan NK, Xu X, Devulder P, et al.
835   SMC5/6 acts jointly with Fanconi anemia factors to support DNA repair and genome
836   stability. *EMBO Rep.* 2020;21(2):e48222.
837   73.   Xue X, Choi K, Bonner JN, Chiba T, Kwon Y, Xu Y, et al. Restriction of replication fork
838   regression activities by a conserved SMC complex. *Mol Cell.* 2014;56(3):436-45.
839   74.   Zapatka M, Pocino-Merino I, Heluani-Gahete H, Bermudez-Lopez M, Tarres M, Ibars E,
840   et al. Sumoylation of Smc5 Promotes Error-free Bypass at Damaged Replication Forks.
841   *Cell Rep.* 2019;29(10):3160-72 e4.
842   75.   Agashe S, Joseph CR, Reyes TAC, Menolfi D, Giannattasio M, Waizenegger A, et al.
843   Smc5/6 functions with Sgs1-Top3-Rmi1 to complete chromosome replication at natural
844   pause sites. *Nat Commun.* 2021;12(1):2111.
845   76.   Albuquerque CP, Wang G, Lee NS, Kolodner RD, Putnam CD, and Zhou H. Distinct
846   SUMO ligases cooperate with Esc2 and Slx5 to suppress duplication-mediated genome
847   rearrangements. *PLoS Genet.* 2013;9(8):e1003670.
848   77.   Misenko SM, and Bunting SF. Rapid analysis of chromosome aberrations in mouse B
849   lymphocytes by PNA-FISH. *J Vis Exp.* 2014(90).
850   78.   Her J, Jeong YY, and Chung IK. PIAS1-mediated sumoylation promotes STUbL-
851   dependent proteasomal degradation of the human telomeric protein TRF2. *FEBS Lett.*
852   2015;589(21):3277-86.
853   79.   Sharma P, Mullen JR, Li M, Zaratiegui M, Bunting SF, and Brill SJ. A Lysine Desert
854   Protects a Novel Domain in the Slx5-Slx8 SUMO Targeted Ub Ligase To Maintain
855   Sumoylation Levels in Saccharomyces cerevisiae. *Genetics.* 2017;206(4):1807-21.
856   80.   Rojas-Fernandez A, Plechanovova A, Hattersley N, Jaffray E, Tatham MH, and Hay RT.
857   SUMO chain-induced dimerization activates RNF4. *Mol Cell.* 2014;53(6):880-92.
858   81.   Bindra RS, Goglia AG, Jasin M, and Powell SN. Development of an assay to measure
859   mutagenic non-homologous end-joining repair activity in mammalian cells. *Nucleic Acids*
860   *Res.* 2013;41(11):e115.
861   82.   Her J, Ray C, Altshuler J, Zheng H, and Bunting SF. 53BP1 Mediates ATR-Chk1
862   Signaling and Protects Replication Forks under Conditions of Replication Stress. *Mol*
863   *Cell Biol.* 2018;38(8).
864   83.   Sleat DE, Della Valle MC, Zheng H, Moore DF, and Lobel P. The mannose 6-phosphate
865   glycoprotein proteome. *J Proteome Res.* 2008;7(7):3010-21.

866   84.   Sleat DE, Lackland H, Wang Y, Sohar I, Xiao G, Li H, and Lobel P. The human brain
867   mannose 6-phosphate glycoproteome: a complex mixture composed of multiple isoforms
868   of many soluble lysosomal proteins. *Proteomics.* 2005;5(6):1520-32.
869   85.   Craig R, and Beavis RC. TANDEM: matching proteins with tandem mass spectra.
870   *Bioinformatics.* 2004;20(9):1466-7.
871   86.   Demichev V, Messner CB, Vernardis SI, Lilley KS, and Ralser M. DIA-NN: neural
872   networks and interference correction enable deep proteome coverage in high throughput.
873   *Nat Methods.* 2020;17(1):41-4.
874   87.   Cox J, Hein MY, Luber CA, Paron I, Nagaraj N, and Mann M. Accurate proteome-wide
875   label-free quantification by delayed normalization and maximal peptide ratio extraction,
876   termed MaxLFQ. *Mol Cell Proteomics.* 2014;13(9):2513-26.
877   88.   Hoadley KA, Yau C, Hinoue T, Wolf DM, Lazar AJ, Drill E, et al. Cell-of-Origin
878   Patterns Dominate the Molecular Classification of 10,000 Tumors from 33 Types of
879   Cancer. *Cell.* 2018;173(2):291-304 e6.
880   89.   Chandrashekar DS, Bashel B, Balasubramanya SAH, Creighton CJ, Ponce-Rodriguez I,
881   Chakravarthi B, and Varambally S. UALCAN: A Portal for Facilitating Tumor Subgroup
882   Gene Expression and Survival Analyses. *Neoplasia.* 2017;19(8):649-58.
883

884
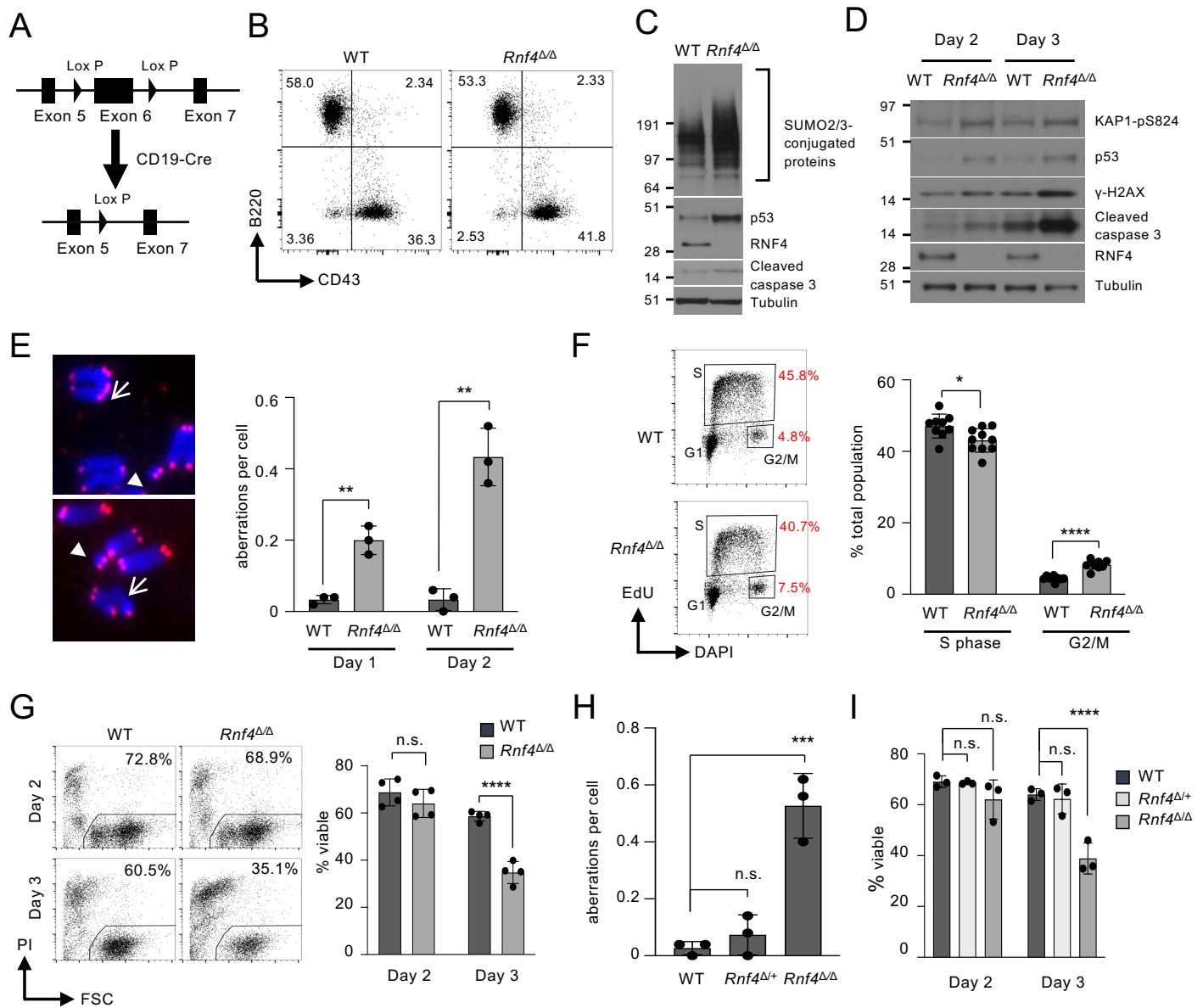
Figure 1. Genomic instability and apoptosis in RNF4 conditional-knockout B cells. (**A**) Schematic representation of Cre-induced deletion of *Rnf4* exon 6. (**B**) Flow cytometry analysis of cell populations in the spleens of WT and *Rnf4*-conditional-knockout (*Rnf4*$^{\Delta/\Delta}$) mice. (**C**) Western blot analysis of protein expression in *Rnf4*$^{\Delta/\Delta}$ B cells after 2 days activation in vitro. (**D**) Western blot to measure induction of markers of DNA damage signaling in activated WT and *Rnf4*$^{\Delta/\Delta}$ B cells after 2 days and 3 days of in vitro culture. (**E**) Analysis of chromosome aberrations in metaphase spreads prepared from WT and *Rnf4*$^{\Delta/\Delta}$ B cells after one or two days of in vitro culture. White arrows show examples of chromosome rearrangements and solid arrowheads show examples of chromosome breaks. (**F**) Cell cycle analysis of fixed B cells after 48 hrs activation in vitro. (**G**) Flow cytometry analysis of cell death in splenic B cells cultured for 2 or 3 days in vitro. Left, figures indicate the percentage of cells that remained viable, based on propidium iodide exclusion. (**H**) Chromosome aberrations in metaphase spreads from WT, *Rnf4*$^{\Delta/+}$, and *Rnf4*$^{\Delta/\Delta}$ B cells. (**I**) Viability of B cells after 2 and 3 days of in vitro culture, measured by DAPI exclusion. Error bars where shown indicate S.D. of the mean. P values were calculated with unpaired t-test (**E**, **F**, **G**), one-way ANOVA with Dunnett's multiple comparisons test (**H**), and two-way ANOVA with Dunnett's multiple comparisons test (**I**).
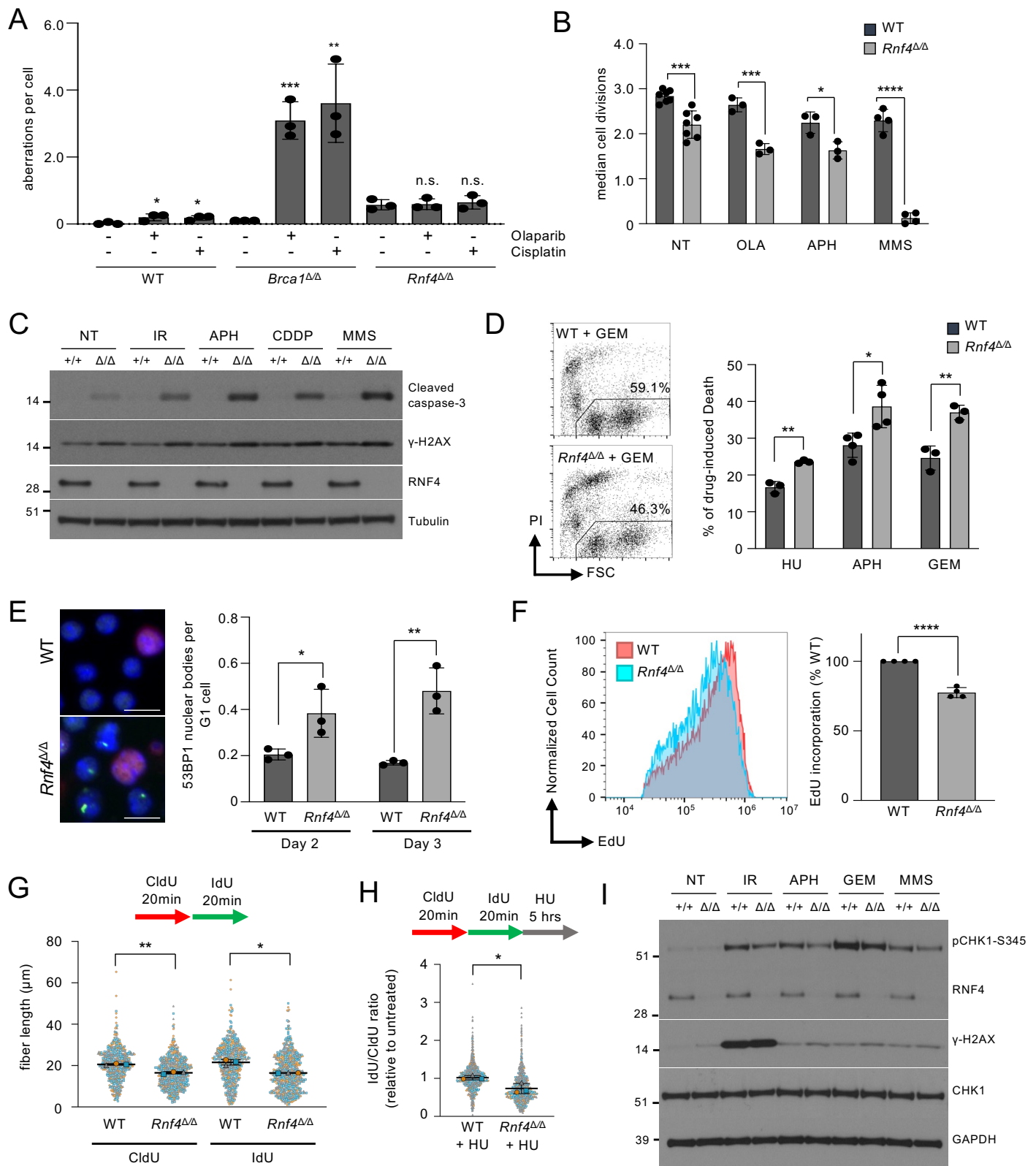
Figure 2. *Rnf4*^Δ/Δ B cells show defects in DNA replication. (**A**) Analysis of chromosome aberrations in B lymphocytes treated overnight ± 2 μM olaparib or 1 μM cisplatin. Statistical differences between the means of the treated and non-treated samples are shown. (**B**) Flow cytometry analysis of CFSE dilution to measure B cell growth over 72 hrs. Chart shows quantification of cell doublings based on CFSE fluorescence. (**C**) Western blot analysis of caspase-3 cleavage and γ-H2AX after no treatment (NT), or after overnight recovery from treatment with 2 Gy of ionizing radiation (IR), 0.4 μM aphidicolin (APH), 2.5 μM cisplatin (CDDP), or 100 μM MMS. (**D**) Sample flow cytometry data quantifying cell viability after treatment with gemcitabine (GEM). Gated population shows the viable, PI-negative population. Graph shows proportion of cells that became non-viable 24 hrs post-treatment with either hydroxyurea (HU) (4 mM, 3 hrs), APH (40 μM, 2 hrs), or GEM (250 nM, 2 hrs). (**E**) Immunofluorescent detection of 53BP1 G1 nuclear bodies (green) in B cells after in vitro culture. Cyclin A staining (red) reveals S/G2-phase cells. (**F**) EdU uptake measured by flow cytometry. (**G**) Analysis of nascent DNA tract length in WT and *Rnf4*^Δ/Δ splenic B cells by DNA combing. Mean ± S.D. of n=3 experiments shown. (**H**) Stability of nascent DNA measured by fiber analysis after 4mM HU treatment. Mean ± S.D. of n=3 experiments shown. (**I**) Western blot to show induction of pCHK1 in WT and *Rnf4*^Δ/Δ cells after IR (30Gy, 2hrs recovery), APH (0.4 μM, overnight), GEM (100 nM, 2 hrs), MMS (200 μM, 3 hrs). Error bars in Parts **A**, **B**, **D**, **E**, and **F** show S.D. of the mean, with P values calculated by unpaired t-test. P values in Parts **G** and **H** calculated by paired t-test.
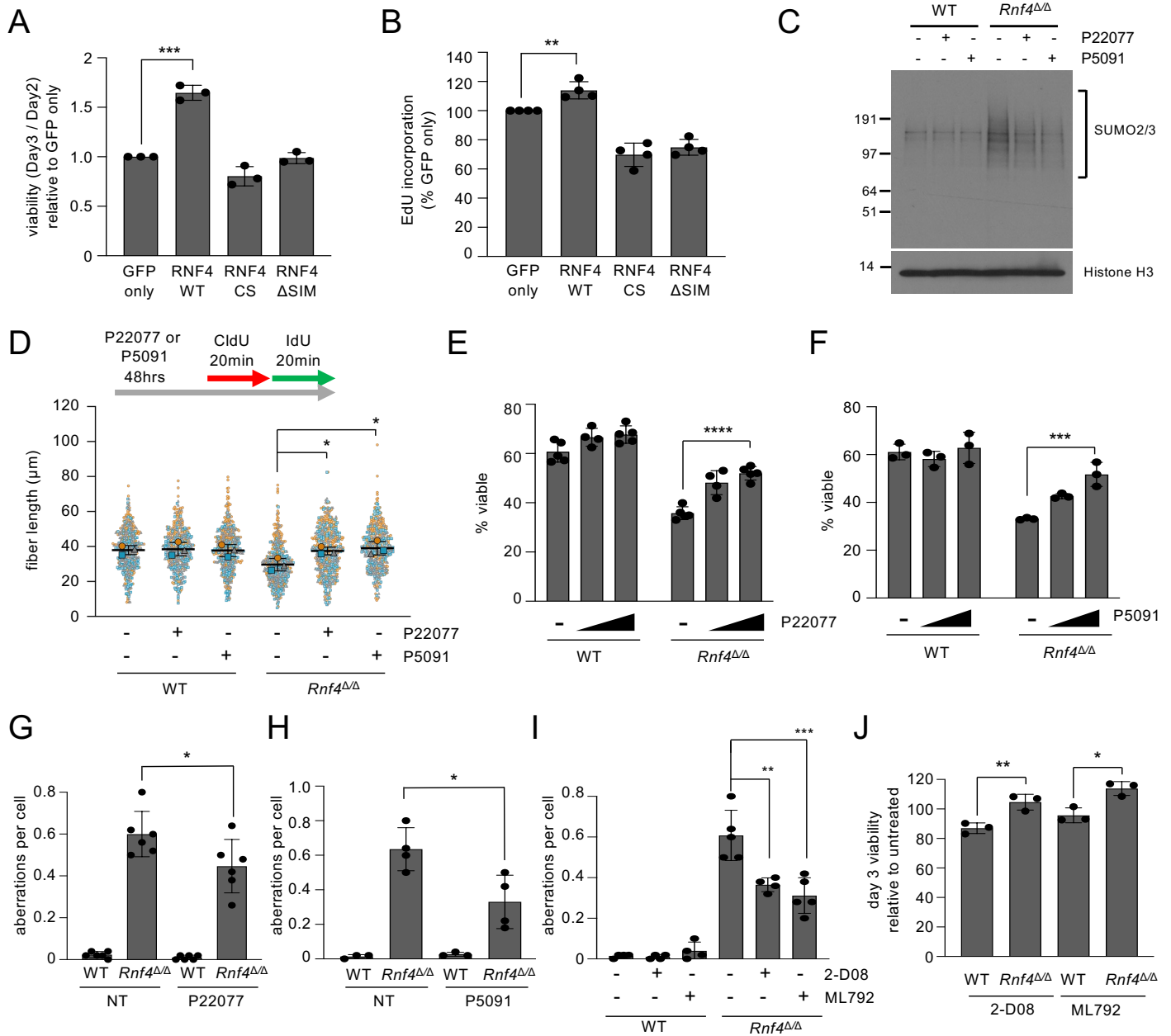
Figure 3. Phenotypes of *Rnf4*^{Δ/Δ} cells are caused by accumulation of SUMOylated proteins (**A**) Analysis of viability of *Rnf4*^{Δ/Δ} cells transduced with constructs expressing GFP, WT RNF4, a catalytic mutant of RNF4 (RNF4-CS) or RNF4 defective for SUMO binding (RNF4-ΔSIM). (**B**) Quantification of EdU uptake by *Rnf4*^{Δ/Δ} cells transduced with GFP or RNF4 cDNAs. (**C**) Western blot of cells grown in vitro for two days ± continual treatment with USP7 inhibitors, P22077 (2 μM) or P5091 (1 μM). (**D**) Analysis of nascent DNA tract length in WT and *Rnf4*^{Δ/Δ} B cells. Cells were cultured in vitro for 48 hrs ± P22077 (2 μM) or P5091 (1 μM), then incubated with CldU for 20 min, followed by IdU for 20 min. CldU and IdU tract lengths were analyzed after DNA combing. Mean ± S.D. of n=3 experiments shown. (**E**) Cell viability after 72 hrs culture ± P22077 (1 μM, 2 μM). Viable cells were identified based on ability to exclude DAPI. (**F**) As (**E**), using P5091 (0.5 μM, 1 μM). (**G**) Analysis of chromosome aberrations in B cells cultured 48 hrs ± P22077 treatment (2 μM). (**H**), as (**G**), using P5091 (1 μM). (**I**) Analysis of chromosome aberrations in B cells cultured 48 hrs ± continuous treatment with the SUMO inhibitors, 2-D08 (40 μM) or ML-792 (20 nM). (**J**) Cell viability measured by quantification of DAPI-negative cells after 72 hrs culture ± 2-D08 (40 μM) or ML-792 (20 nM). Error bars in parts **A**, **B**, and **E-J**, show S.D. of the mean. P values were calculated with unpaired t-test (**A**, **B**, **J**), one-way ANOVA with Dunnett's multiple comparison test, (**D**, **I**), two-way ANOVA with Dunnett's multiple comparison test (**E**, **F**), and one-way ANOVA with Tukey's multiple comparison test (**G**, **H**).
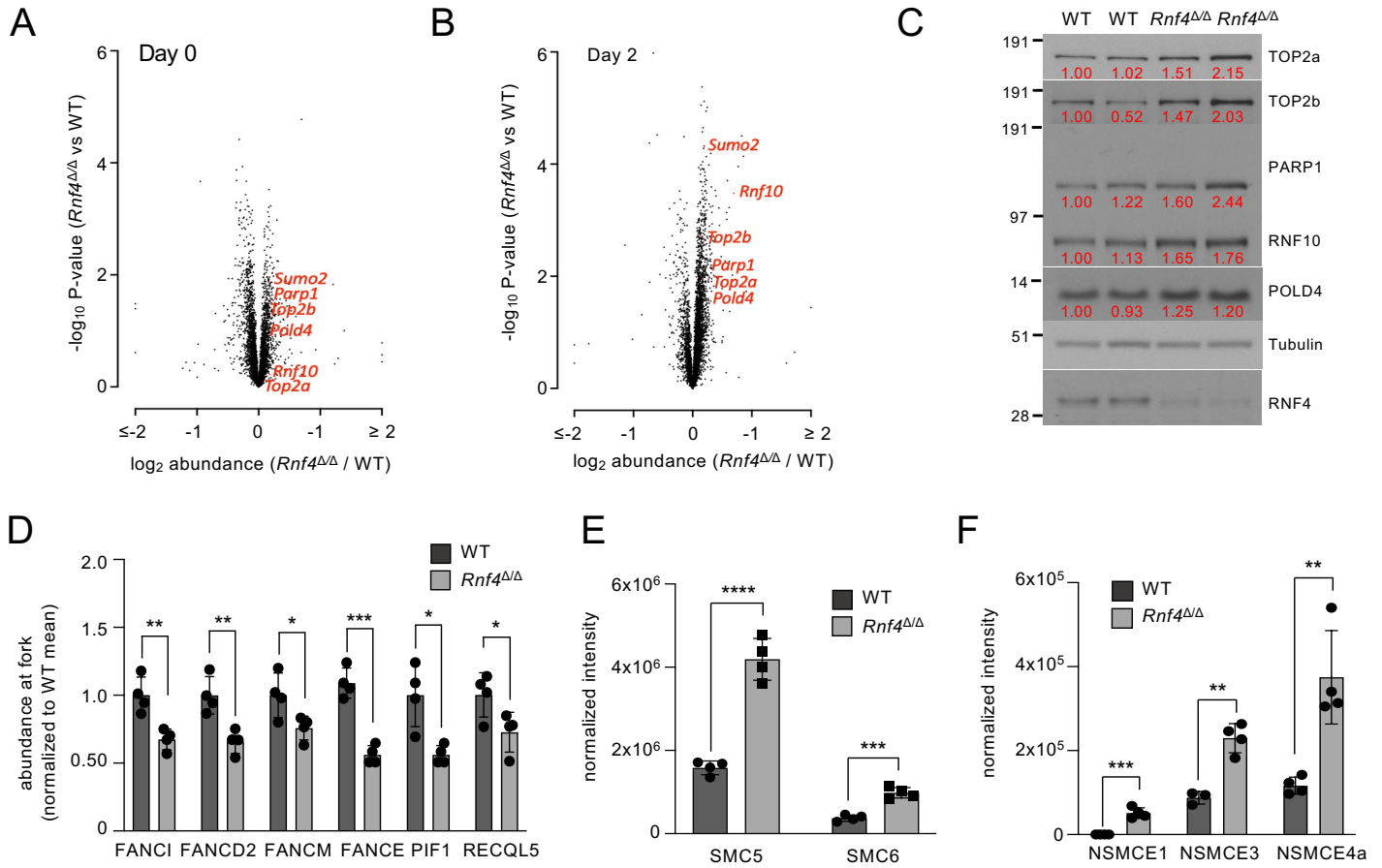
Figure 4: RNF4 deficiency leads to reduced accumulation of proteins needed for replication stress responses at replication forks. (**A**) Volcano plot showing protein abundance in resting $Rnf4^{\Delta/\Delta}$ B cells relative to WT controls. Each data point represents the average of four samples. Six proteins that showed increased abundance after B cell activation are labeled. (**B**) Volcano plot of B cells after 48 hrs in vitro culture with cell proliferation induced by addition of LPS. (**C**) Western blot showing expression of proteins in WT and $Rnf4^{\Delta/\Delta}$ B cells after 48 hrs culture. Two samples are shown in each case. Figures in red indicate band intensities measured with ImageJ. (**D**) Abundance of proteins required for replication stress responses at replication forks, measured by iPOND-MS, in WT and $Rnf4^{\Delta/\Delta}$ B cells. (**E**) Increase in abundance of SUMOylated SMC5 and SMC6 in $Rnf4^{\Delta/\Delta}$ cells, measured by mass spectrometry after SUMO2/3 immunoprecipitation of chromatin from WT and $Rnf4^{\Delta/\Delta}$ cells. (**F**) Increase in abundance of SUMOylated Non-SMC Element (NSMCE) subunits of the SMC5/6 complex in chromatin of $Rnf4^{\Delta/\Delta}$ cells. Error bars in parts **D-F** show S.D. of the mean of n=4 replicates. P values were calculated by unpaired t-test. P < 0.05 was considered significant.
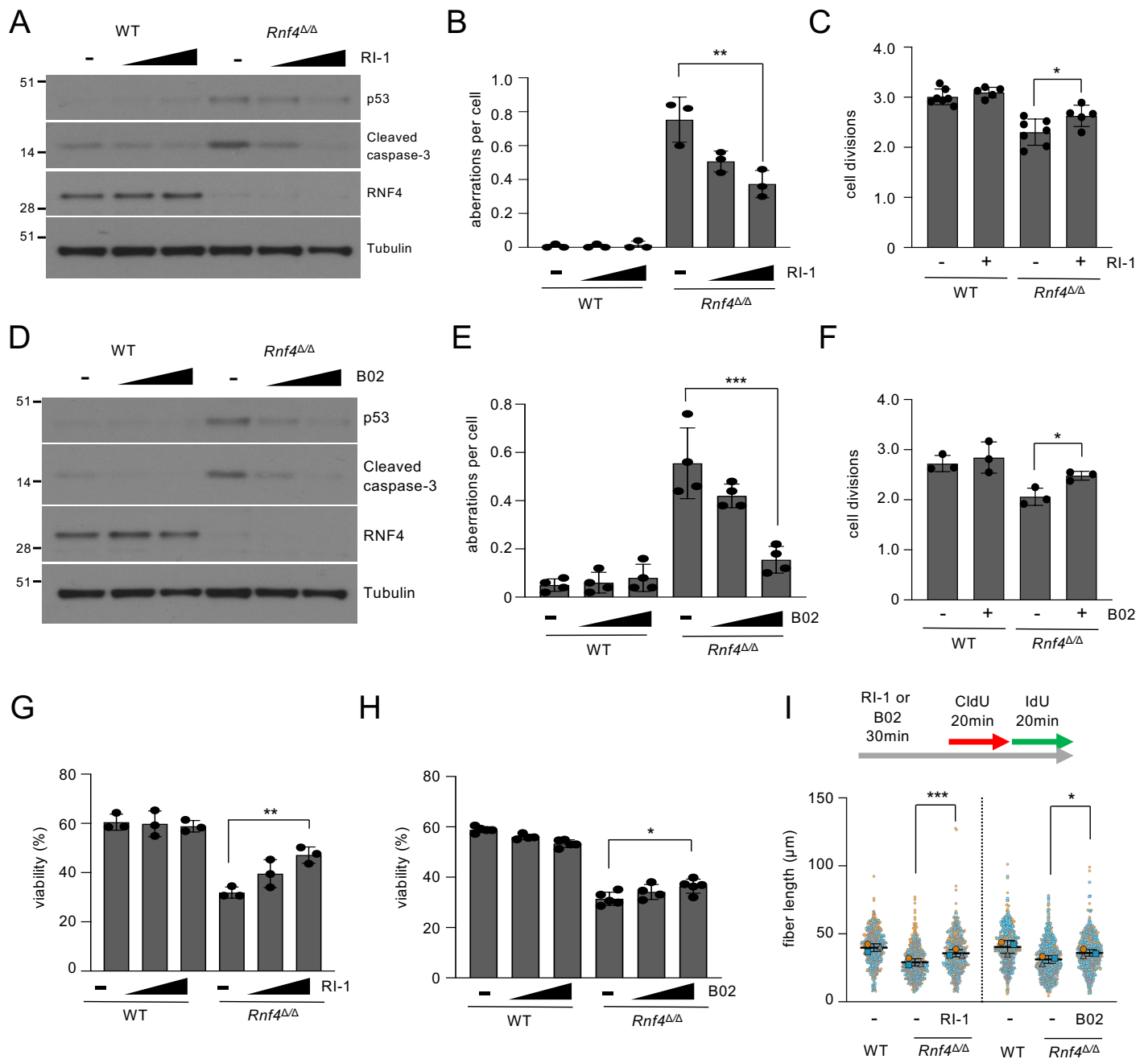
Figure 5: Genomic instability and cell death in RNF4-deficient cells is dependent on RAD51. (**A**) Western blot analysis of WT and *Rnf4^{Δ/Δ}* B cells cultured in vitro for 72 hrs with mock treatment (-) or with the RAD51 inhibitor, RI-1 (5 μM, 10 μM). (**B**) Analysis of chromosome aberrations in Day 2 cultured B cells ± RI-1 treatment (5 μM, 10 μM). (**C**) Analysis of CFSE FACS to measure cell proliferation during 72 hrs growth ± RI-1 treatment (5 μM). (**D**) As (**A**) with the RAD51 inhibitor, B02 (5 μM, 10 μM). (**E**) As (**B**), with B02 (5 μM, 10 μM). (**F**) As (**C**) with B02 (5 μM). (**G**) Viability of B cells, measured by DAPI exclusion, after treatment with RI-1 (5 μM, 10 μM) on Day 3. (**H**) As (**G**) with B02 (2.5 μM, 5 μM). (**I**) Measurement of newly-replicated DNA by DNA combing after pulsing cells with CldU and IdU ± RI-1 or B02 (10 μM in each case). Mean ± S.D. of n=3 experiments shown. Error bars in parts **B-C** and **E-H** represent S.D. of the mean. P values were calculated by one-way ANOVA with Dunnett's multiple comparison test (**B**, **E**, **G**, **H**), unpaired t-test (**C**, **F**), and one-way ANOVA with Tukey's multiple comparison test (**I**). P < 0.05 was considered significant.
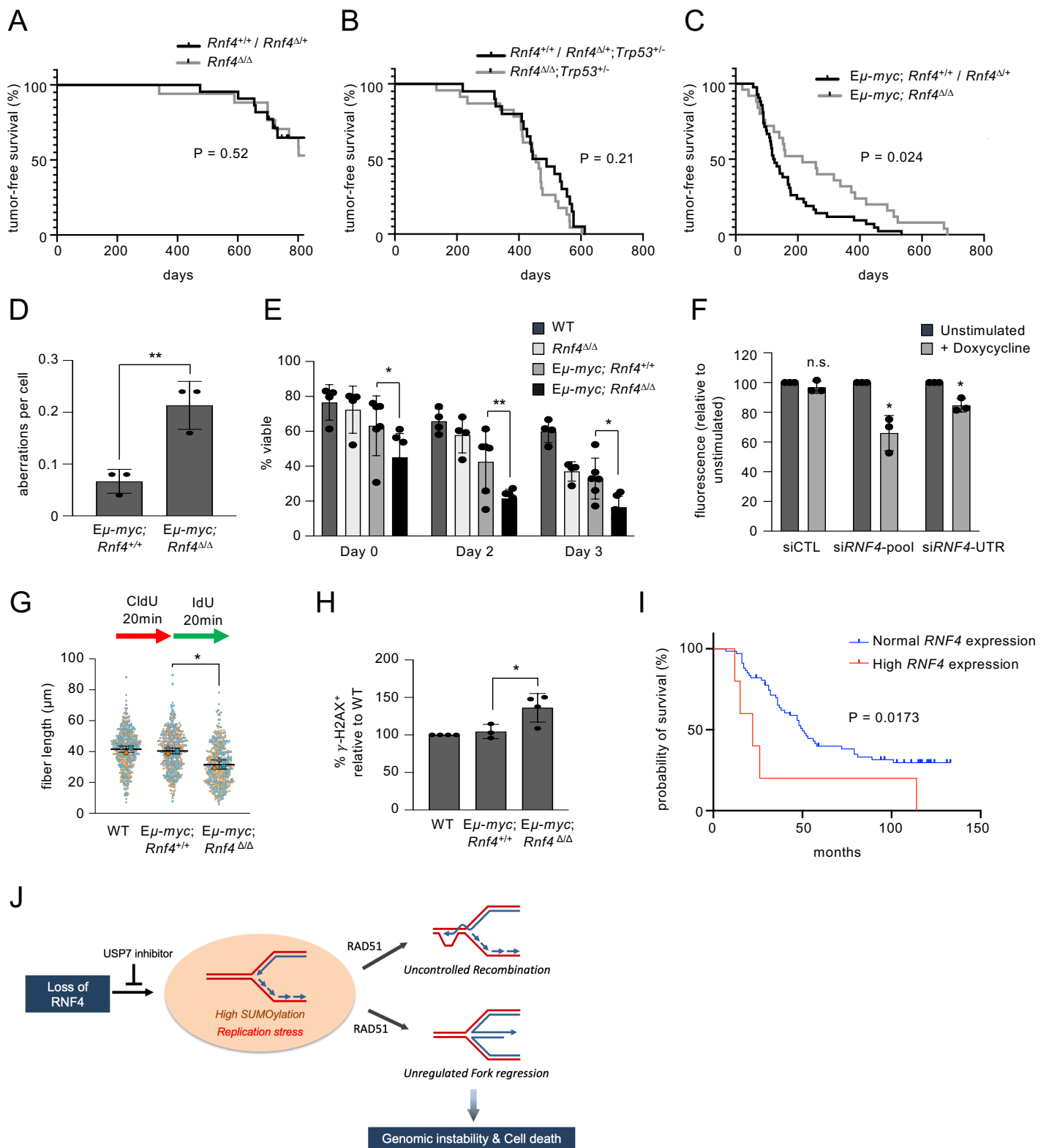
Figure 6: RNF4 deficiency extends tumor-free lifespan of Eµ-myc transgenic mice. (**A**) Tumor-free survival of *Rnf4⁺/⁺;CD19-Cre* or *Rnf4^f/f^;CD19-Cre* (n = 38), and *Rnf4^f/f^;CD19-Cre* (n = 44). (**B**) Tumor-free survival of *Rnf4⁺/⁺;Trp53⁺/⁻;CD19-Cre* or *Rnf4^f/+^;Trp53⁺/⁻;CD19-Cre* (n = 30), and *Rnf4^f/f^;Trp53⁺/⁻;CD19-Cre* (n = 30). (**C**) Tumor-free survival of Eµ-myc;*Rnf4⁺/⁺;CD19-Cre* or Eµ-myc;*Rnf4^f/+^;CD19-Cre* (n = 47), and Eµ-myc;*Rnf4^f/f^;CD19-Cre* (n = 27). (**D**) Analysis of chromosome aberrations of B cells of the indicated genotypes after two days in culture. (**E**) Analysis of cell viability of B cells of the indicated genotypes during 72 hrs of in vitro growth. (**F**) Growth of U2OS-iMYC cells after doxycycline-induced expression of c-*myc*, measured by quantification of CellTiterGlo fluorescence. P values show difference between the means of unstimulated and stimulated cells. (**G**) Analysis of replication fork velocity measured by DNA combing. Total CldU + IdU tract length is shown. Mean ± S.D. of n=3 experiments shown. (**H**) % of S-phase (EdU⁺) cells staining positively for γ-H2AX. (**I**) Survival of pediatric B cell acute lymphoblastic leukemia (B-ALL) patients with tumors expressing either normal or increased levels of *RNF4*. (**J**) Model for steps leading to cell death in RNF4-deficient cells. Absence of RNF4 activity causes increased abundance of SUMOylated proteins in chromatin, leading to replication stress and accumulation of non-productive intermediates, dependent on RAD51, which prevents successful completion of DNA replication and further cell proliferation. Error bars in parts **D-F**, and **H** show S.D. of the mean. P values were calculated by log-rank test (**A-C**, **I**), unpaired t-test (**D**, **F**), two-way ANOVA with Dunnett's multiple comparison test (**E**), and one-way ANOVA with Tukey's multiple comparison test (**G**, **H**). P < 0.05 was considered statistically significant.
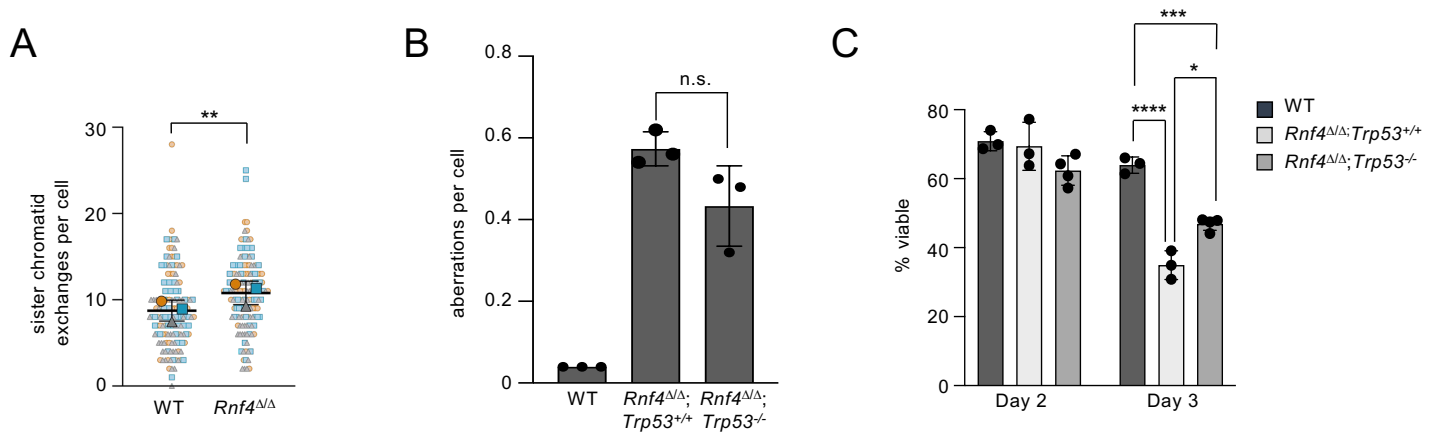
Supplemental Figure 1: (**A**) Quantification of sister chromatid exchanges in WT and $Rnf4^{\Delta/\Delta}$ B cells after 48 hrs growth in vitro. Mean $\pm$ S.D. of n=3 experiments shown. (**B**) Quantification of metaphase chromosome aberrations from B cells of the indicated genotypes. Error bars show S.D. of the mean. (**C**) Viability of B cells of the indicated genotypes after two or three days in culture. Viable cells were identified by FACS on the basis of PI exclusion. P values were calculated by paired t-test (**A**), unpaired t-test (**B**), and two-way ANOVA with Tukey's multiple comparison test (**C**). $P < 0.05$ was considered significant.
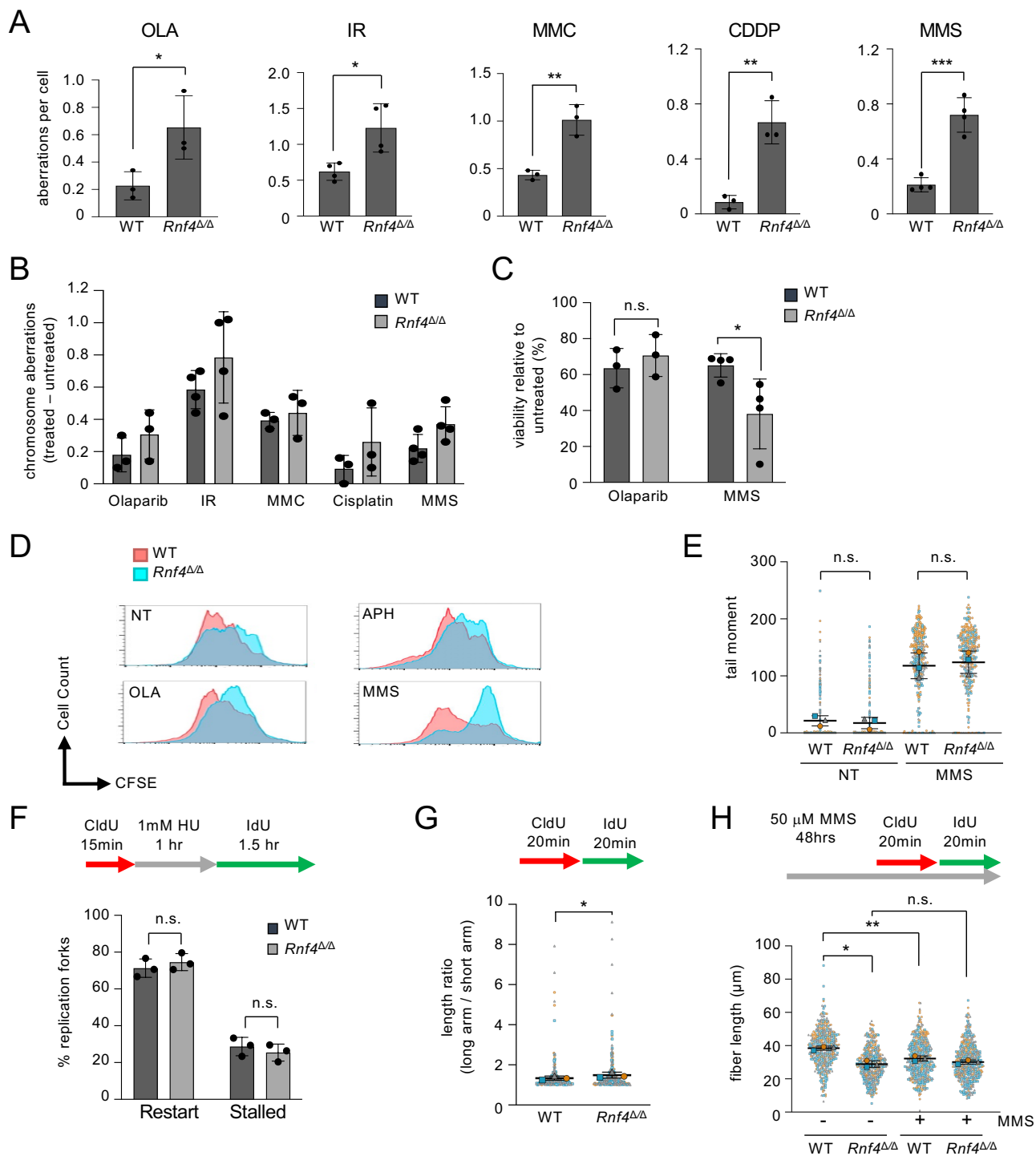
Supplemental Figure 2: (**A**) Chromosome aberrations in WT and $Rnf4^{\Delta/\Delta}$ B cells cultured for 36 hrs in vitro followed by overnight treatment with either olaparib (2 μM), ionizing radiation (2 Gy), mitomycin C (MMC, 250 nM), cisplatin (1 μM), or methyl methanesulfonate (MMS, 100 μM). (**B**) Total chromosome aberrations induced by treatments as shown in (A), after subtracting the number of chromosome aberrations present in untreated WT and $Rnf4^{\Delta/\Delta}$ B cells. The differences between the means did not meet the threshold for statistical significance (P < 0.05) in any case. (**C**) B cell viability after induction of DNA damage. B cells were grown for 72 hrs in culture ± olaparib (1 μM) or MMS (100 μM). Viability was measured by flow cytometry based on DAPI exclusion. (**D**) Representative data for Figure 2B, flow cytometry analysis of CFSE dilution to measure B cell growth in vitro over 72 hrs. (**E**) Alkaline comet assay to measure single-strand DNA breaks in cells of the indicated genotypes after 2 days in culture. MMS treatment was 100 μM, 3 hrs. Mean ± S.D. of n=3 experiments shown. (**F**) DNA fiber analysis to measure fork stalling and restart after hydroxyurea treatment. (**G**) Measurement of asymmetry of replication from single replication origins, measured by DNA fiber analysis. The ratio of the longer replication tract compared to the shorter tract was quantified for each origin. Mean ± S.D. of n=3 experiments shown. (**H**) Measurement of replication fork velocity by DNA combing in untreated cells and after treatment with MMS. Mean ± S.D. of n=3 experiments shown. For parts **A-C** and **F**, error bars represent the S.D. of the means. P values were calculated by unpaired t-test (**A-C**, **F**), paired t-test (**E**, **G**), and one-way ANOVA with Tukey's multiple comparison test (**H**). P <0.05 was considered statistically significant.
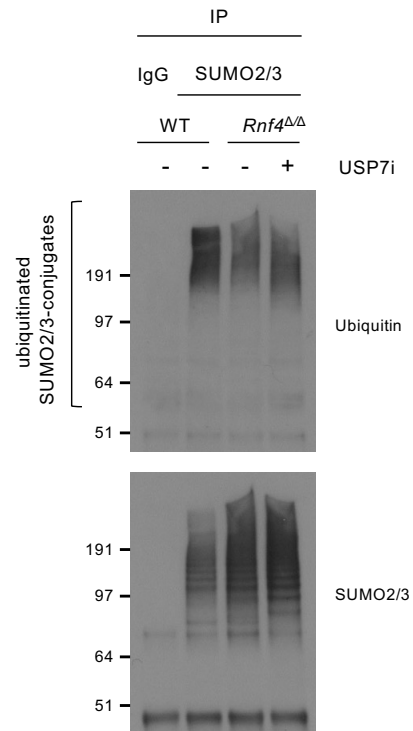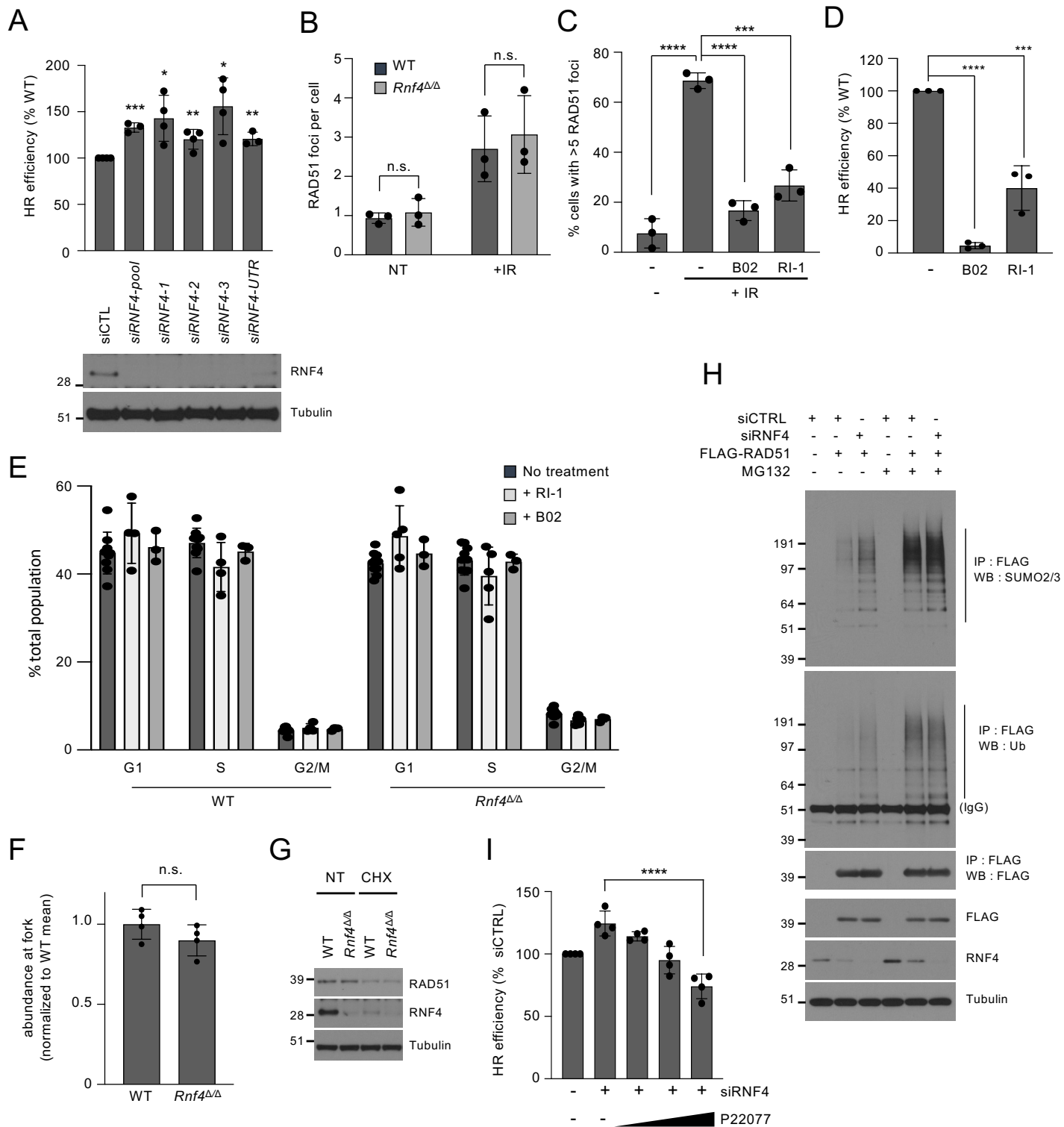
Supplemental Figure 3: Western blot to measure levels of ubiquitination of SUMO-conjugated proteins on chromatin in *Rnf4*$^{\Delta/\Delta}$ B cells after short-term treatment with USP7 inhibitor. B cells cultured in vitro for 48 hrs were either untreated (-) or treated with 50 μM P22077 for 4 hrs. SUMO2/3-conjugates were immunoprecipitated from the chromatin fraction of B cells using an anti-SUMO2/3 antibody, and subsequently used for detection of ubiquitin.
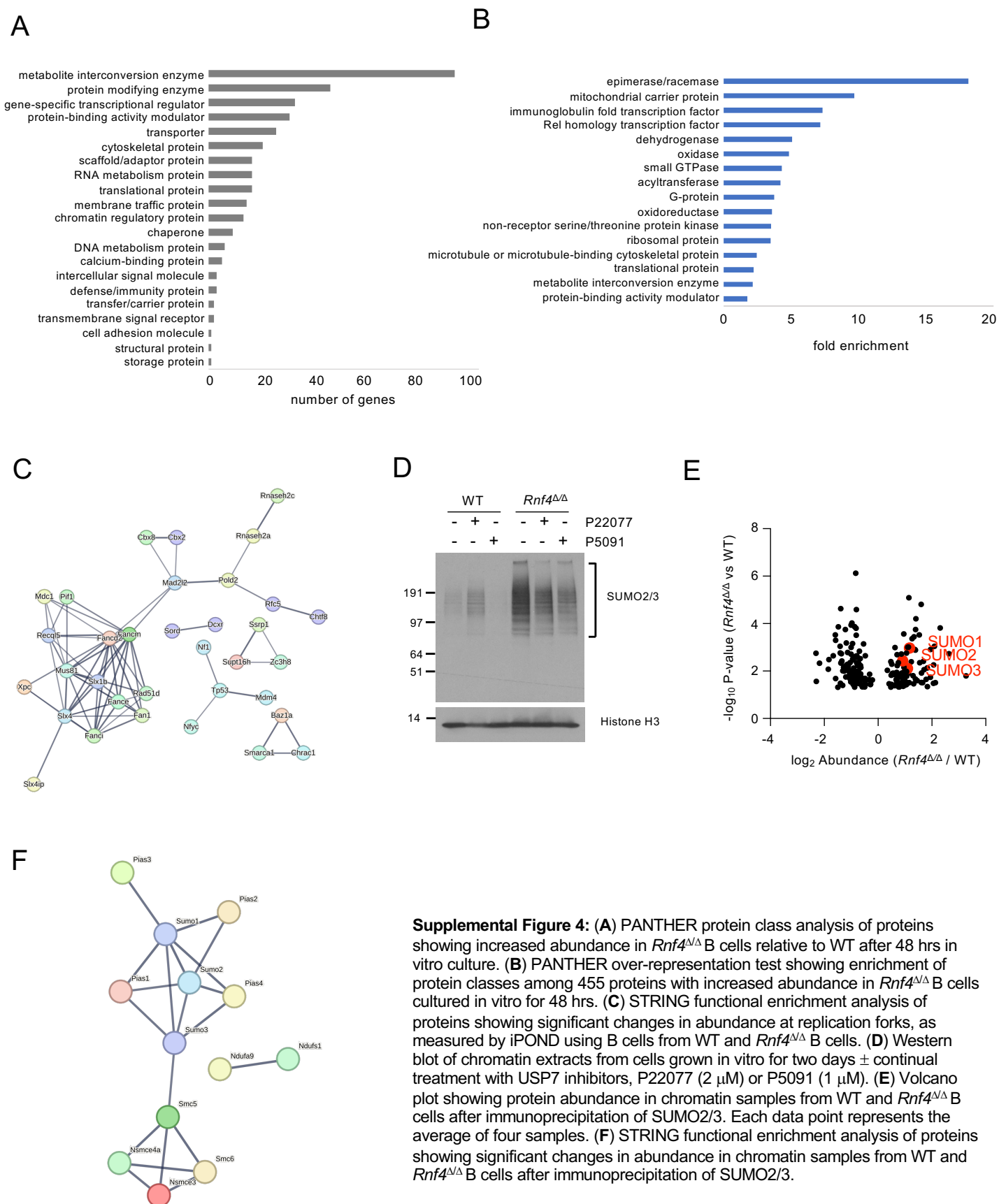
Supplemental Figure 4: (**A**) PANTHER protein class analysis of proteins showing increased abundance in $Rnf4^{\Delta/\Delta}$ B cells relative to WT after 48 hrs in vitro culture. (**B**) PANTHER over-representation test showing enrichment of protein classes among 455 proteins with increased abundance in $Rnf4^{\Delta/\Delta}$ B cells cultured in vitro for 48 hrs. (**C**) STRING functional enrichment analysis of proteins showing significant changes in abundance at replication forks, as measured by iPOND using B cells from WT and $Rnf4^{\Delta/\Delta}$ B cells. (**D**) Western blot of chromatin extracts from cells grown in vitro for two days ± continual treatment with USP7 inhibitors, P22077 (2 μM) or P5091 (1 μM). (**E**) Volcano plot showing protein abundance in chromatin samples from WT and $Rnf4^{\Delta/\Delta}$ B cells after immunoprecipitation of SUMO2/3. Each data point represents the average of four samples. (**F**) STRING functional enrichment analysis of proteins showing significant changes in abundance in chromatin samples from WT and $Rnf4^{\Delta/\Delta}$ B cells after immunoprecipitation of SUMO2/3.

Supplemental Figure 5: (**A**) Measurement of homologous recombination frequency by DR-GFP assay after transfection with either control siRNA (siCTRL) or siRNA oligonucleotides targeting *RNF4*. Efficiency of knockdown is shown by Western blot in the lower panel. (**B**) Quantification of RAD51 foci in cells after no treatment (NT), or after 4 hrs recovery from treatment with 10 Gy of ionizing radiation (IR). (**C**) Analysis of proportion of WT cells showing >5 ionizing radiation-induced nuclear foci after either no treatment (-) or with the RAD51 inhibitors, B02 and RI-1 (1 hr, 50 μM). (**D**) Homologous recombination efficiency measured by DR-GFP assay in cells that were either untreated (-) or treated for 1 hr with B02 (20 μM) or RI-1 (50 μM). (**E**) Measurement of cell cycle by quantification of EdU incorporation and DAPI binding in splenic B cells after 48 hrs growth in vitro ± 10 μM RI-1 or 5 μM B02. (**F**) Abundance of RAD51 at active replication forks, measured by iPOND-MS in n=4 replicate samples. (**G**) RAD51 abundance measured by Western blot in cells that were either not treated (NT) or treated with 25 μg/ml cycloheximide (CHX) for 4 hrs. (**H**) Analysis of ubiquitin present in FLAG-RAD51 pulldown samples in cells treated with either control siRNA (siCTRL) or siRNA targeting RNF4 (siRNF4). Some samples were treated with the proteasome inhibitor, MG132 (10 μM, 4 hrs). (**I**) Homologous recombination efficiency measured by DR-GFP in cells that were treated ± siRNF4 and /or the USP7 inhibitor, P22077 (2, 5, 10μM). Error bars in **A-F**, and **I** represent the S.D. of the mean. P values were calculated by unpaired t-test (**A**, **B**, **F**), one-way ANOVA with Tukey's multiple comparison test (**C**, **I**), and one-way ANOVA with Dunnett's multiple comparison test (**D**). P < 0.05 was considered significant.
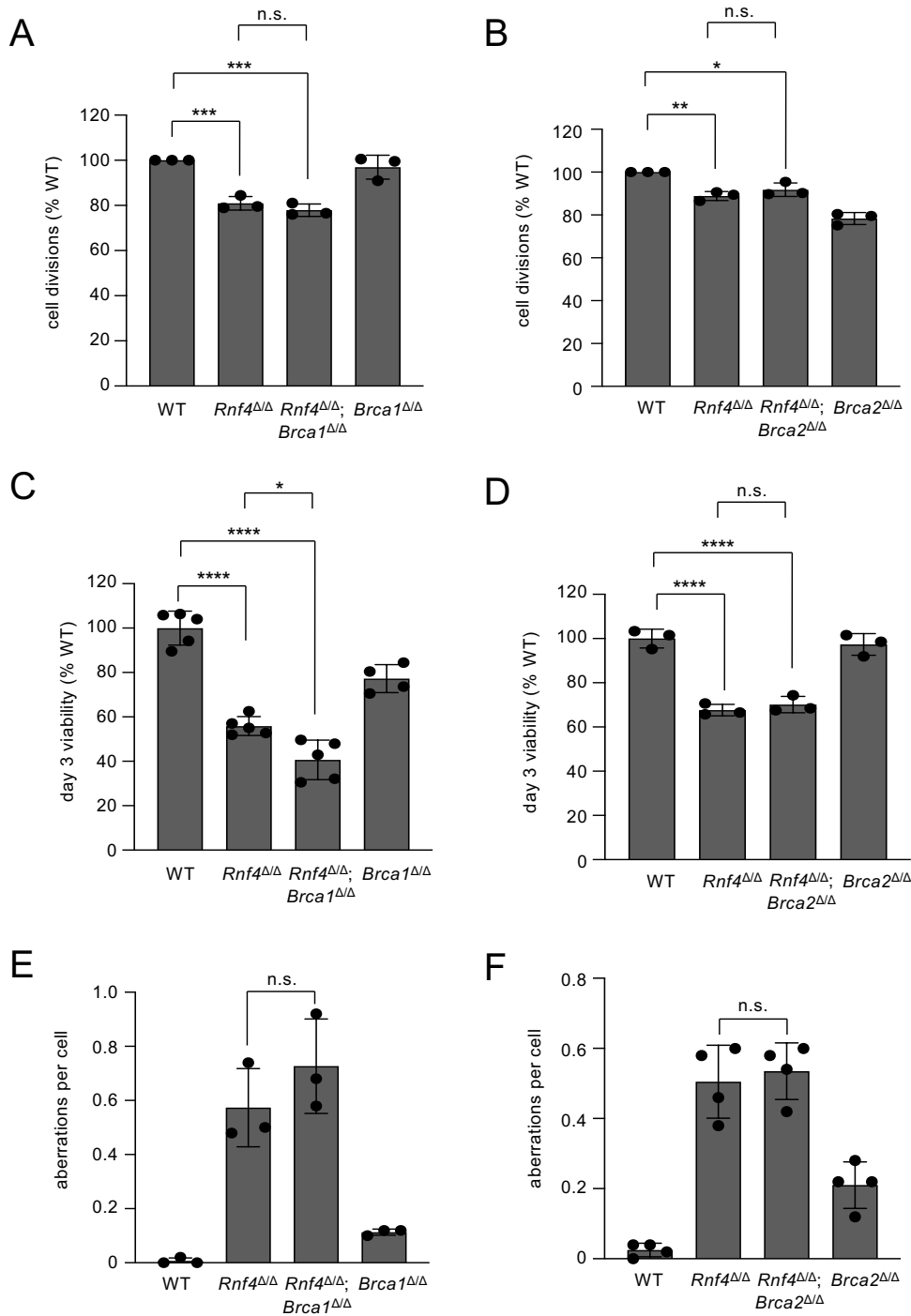
Supplemental Figure 6: (**A**) Quantification of proliferation of B cells growing in vitro for 72 hrs, measured by flow cytometry analysis of CFSE dilution. *Rnf4* and *Brca1* were deleted either singly or in combination in the B cell lineage by breeding to a CD19-Cre transgenic line. (**B**) as (**A**) but with conditional deletion of *Brca2* on a WT or *Rnf4*$^{\Delta/\Delta}$ background. (**C**) Quantification of cell viability of cells of the indicated genotypes, after three days of in vitro B cell culture. Cell viability was measured by DAPI exclusion, as detected by flow cytometry. (**D**) As (**C**) but with deletion of *Brca2*. (**E**) Quantification of chromosome aberrations of B cells of the indicated genotypes. (**F**) As (**E**) but with conditional deletion of *Brca2*. Error bars show the S.D. of the mean in each case, with P values calculated by one-way ANOVA with Tukey's multiple comparison test. A P value < 0.05 was considered statistically significant.
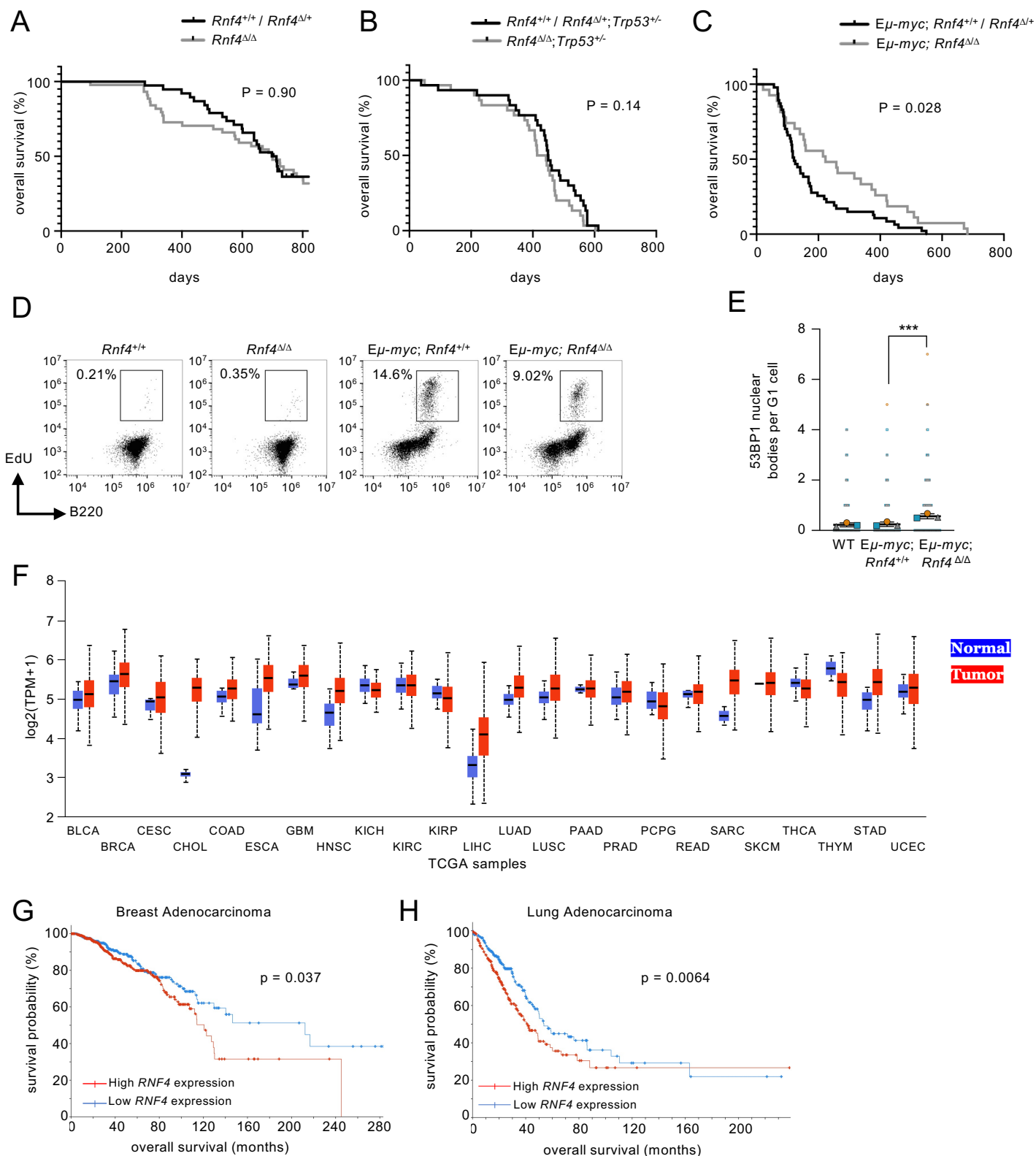
Supplemental Figure 7: (**A**) Kaplan-Meier analysis showing overall survival of $Rnf4^{+/+};CD19\text{-}Cre$ or $Rnf4^{f/+};CD19\text{-}Cre$ (n = 38), and $Rnf4^{f/f};CD19\text{-}Cre$ (n = 44). (**B**) Kaplan-Meier analysis of overall survival of $Rnf4^{+/+};Trp53^{+/-};CD19\text{-}Cre$ or $Rnf4^{f/+};Trp53^{+/-};CD19\text{-}Cre$ (n = 30), and $Rnf4^{f/f};Trp53^{+/-};CD19\text{-}Cre$ (n = 30). (**C**) Kaplan-Meier analysis of overall survival of Eμ-myc;$Rnf4^{+/+};CD19\text{-}Cre$ or Eμ-myc;$Rnf4^{f/+};CD19\text{-}Cre$ (n = 47), and Eμ-myc;$Rnf4^{f/f};CD19\text{-}Cre$ (n = 27). (**D**) Flow cytometry analysis showing EdU uptake by B220$^+$ resting B cells from the spleens of WT, $Rnf4^{\Delta/\Delta}$, and Eμ-myc transgenic mice. (**E**) Quantification of 53BP1 G1 nuclear bodies, measured by anti-53BP1 immunofluorescence in G1 cells of the indicated genotypes after two days of in vitro culture. P value calculated with Mann-Whitney U-test. Mean ± S.D. of n=3 experiments shown. (**F**) Expression of $RNF4$ in different tumor types according to TCGA data sets. (**G**) Survival of breast adenocarcinoma patients with tumors expressing either above-median (n = 541) or below-median (n = 541) levels of RNF4. Data from TCGA PanCancer Atlas retrieved through cBioPortal. (**H**) Survival of patients with lung adenocarcinoma expressing either above-median (n = 249) or below-median (n = 252) levels of RNF4. P values in **A-C** and **G-H** calculated by log-rank test. P value in **E** calculated by paired t-test. P < 0.05 was considered significant in each case.